TOPICAL REVIEW • OPEN ACCESS

A brief review on the recent development of phonon engineering and manipulation at nanoscales

To cite this article: Siqi Xie *et al* 2024 *Int. J. Extrem. Manuf.* **6** 012007

OPEN ACCESS
IOP Publishing | IMMT
International Journal of Extreme Manufacturing
Int. J. Extrem. Manuf. **6** (2024) 012007 (30pp)
https://doi.org/10.1088/2631-7990/acfd68

Topical Review

A brief review on the recent development of phonon engineering and manipulation at nanoscales

Siqi Xie, Hongxin Zhu, Xing Zhang and Haidong Wang*

Key Laboratory for Thermal Science and Power Engineering of Ministry of Education, Department of Engineering Mechanics, Tsinghua University, Beijing 100084, People's Republic of China

E-mail: hdwang@tsinghua.edu.cn

Received 4 April 2023, revised 30 June 2023
Accepted for publication 25 September 2023
Published 13 October 2023

Abstract

Phonons are the quantum mechanical descriptions of vibrational modes that manifest themselves in many physical properties of condensed matter systems. As the size of electronic devices continues to decrease below mean free paths of acoustic phonons, the engineering of phonon spectra at the nanoscale becomes an important topic. Phonon manipulation allows for active control and management of heat flow, enabling functions such as regulated heat transport. At the same time, phonon transmission, as a novel signal transmission method, holds great potential to revolutionize modern industry like microelectronics technology, and boasts wide-ranging applications. Unlike fermions such as electrons, polarity regulation is difficult to act on phonons as bosons, making the development of effective phonon modulation methods a daunting task. This work reviews the development of phonon engineering and strategies of phonon manipulation at different scales, reports the latest research progress of nanophononic devices such as thermal rectifiers, thermal transistors, thermal memories, and thermoelectric devices, and analyzes the phonon transport mechanisms involved. Lastly, we survey feasible perspectives and research directions of phonon engineering. Thermoelectric analogies, external field regulation, and acousto-optic co-optimization are expected to become future research hotspots.

Keywords: phonon engineering, phononic device, nanoscale

1. Introduction

Phonons are quantized representations of lattice vibrations. Similar to photons, phonons carry the energy and momentum of sound waves. However, they are not real particles in the ordinary sense, but quasi-particles. Suppose the frequency of the lattice wave is ω and the wave vector is q. Then the phonon has quasi-energy $\hbar\omega$ and quasi-momentum $\hbar q$, where $\hbar$ is the Planck constant. The relationship between the phonon frequency and the wave vector is called the phonon dispersion $\omega(q)$, also known as the lattice vibration spectrum. For a unit cell containing n atoms, each wave vector q corresponds to n vibration frequencies, and considering three polarization directions, a total of $3n$ phonon dispersion modes are formed. Among these modes, the three with lower vibration frequencies are acoustic phonon branches, and the corresponding phonons in these branches are called acoustic phonons. The remaining $3(n-1)$ modes are optical phonon branches, and the corresponding phonons are referred to as optical phonons.

* Author to whom any correspondence should be addressed.

2631-7990/24/012007+30$33.00

Acoustic lattice waves exist in all crystals, but optical lattice waves do not exist in simple lattice (non-complex lattice) crystals.

Phonons play pivotal roles in broad physical properties of solid-state materials. For example, phonons and their interactions with other particles limit carrier mobility and electrical conductivity [1–3]. Acoustic phonons are primary heat carriers in semiconductors and insulators [4]. Optical phonons are one of the primary factors affecting optical properties of semiconductors [5]. Therefore, the ability to manipulate phonons holds significant implications for tailoring intrinsic properties of materials. As the development of the silicon-based semiconductor industry has entered a bottleneck, the size of transistors has reached below 3 nm, which is close to the physical limit, and Moore's law has expired. Logic operations based on phonon manipulation, that is, phonon computers, will form a new breakthrough technology and significantly change the existing structure of information industry. Functions such as thermal rectification realized by phonon manipulation are able to effectively enhance the heat dissipation capability of nanoscale devices and further improve the performance of integrated electronic chips. In addition, the development of emerging technologies such as thermal cloaking and thermal metamaterials also provides broad application prospects for phonon manipulation.

Electronic manipulation, for example, diodes, triodes, logic circuits, etc, is the foundation of the modern information industry. Since electrons belong to fermions, the transport properties of electrons can be easily controlled via polarity voltage. Nevertheless, bosonic nature of phonons renders them immune to polarity-based control methods such as electricity, magnetism, and light, which means it is difficult to manipulate the transmission of phonons through existing electronic manipulation methods. In the past few decades, phonon manipulation has been found to be possible by introducing disorder, interfaces, boundaries, defects and asymmetric structures in materials. Using first-principles calculations, Lindsay *et al* [6] reported that the thermal conductivity of isotope-rich boron arsenide exceeded 3000 $\mathrm{Wm^{-1}\cdot K^{-1}}$ at room temperature, equivalent to that in diamonds, which is the highest thermal conductivity known. Large frequency gap between acoustic and optical phonons branches and the aggregation of phonon branches would produce weak anharmonic phonon scattering. This anharmonic scattering together with strong isotope scattering is an important factor contributing to the large isotope effects. Chiritescu *et al* [7] found that disordered, layered WSe_2 crystals had a cross-plane thermal conductivity as small as 0.05 $\mathrm{Wm^{-1}\cdot K^{-1}}$ at room temperature, which was 30 times smaller than that of single-crystal WSe_2 samples. The authors attributed this ultralow thermal conductivity to phonon localization induced by the random stacking of 2D WSe_2 sheets. In addition, the fabrication of phonon devices using phonon modulation methods has also garnered extensive attention among researchers, which can be used for heat transfer, heat control and thermal rectification in nano systems [8]. Chen *et al* [9] studied thermal rectification of asymmetric graphene/h-BN vdW heterostructures by molecular dynamics (MD) simulations. The results showed that the heat flux preferentially flowed in the direction from the monolayer to the multilayer regions, and the rectification ratio could reach up to 37.9%. This phenomenon is probably attributed to the strong suppression of low-frequency out-of-plane phonons of encased graphene under negative temperature bias.

Although scholars have achieved numerous uplifting research outcomes in the field of phonon manipulation in the past few decades, there is a lack of retrospective articles that comprehensively summarize them. This review will furnish a brief overview of the development of phonon engineering, and focus primarily on the latest progress in nanoscale phonon manipulation and the realization of thermal functional devices from the aspects of principles, theories, calculations and experiments (figure 1). This review also provides an outlook on future directions of phonon engineering at the nanoscale. The structural design methods and research tools mentioned in this paper offer clear guidance for future developments and practical applications of phonon engineering, and are helpful to broaden researches on phononic devices and logic-thermal circuits.

2. Phonon engineering

The core idea of phonon engineering is to adjust the phonon dispersion in order to control phonon transport, and further realize the modulation of a certain performance. In this review, thermal phonon engineering is mainly discussed. In 1929, the concept of 'elastic quanta' was introduced by Igor Tamm to describe the quantum energy of lattice vibration [21]. In the same year, Peierls [22] introduced the Boltzmann transport equation to describe heat transport in dielectrics as the motion and scattering of phonon gas with reference to the gas-dynamical model. However, due to the complexity of the phonon Boltzmann equation, it is extremely difficult to obtain its exact solutions, so many scholars introduced assumptions and approximations into the equation in order to acquire simpler calculative expressions for heat transport. In 1958, with relaxation time approximations and the assumption that there is no difference between transverse and longitudinal phonons, Callaway [23] conducted a special investigation on the normal processes which conserve quasi-momentum, and proposed a phenomenological model to calculate low-temperature thermal conductivity, which was in good agreement with the experimental results. Ulteriorly, in 1963, Holland [24] separated contributions of transverse phonons and longitudinal phonons to thermal conductivity according to the available detailed distributions of phonon density of states (DOS), and derived a lattice thermal conductivity expression that was effective in a large range of temperatures and phonon frequencies. He also affirmed the validity of the Callaway model in the regions of impurity scattering and boundary scattering. These models are still widely used in the researches of thermal characteristics of various materials, and many modified models have been proposed one after another. Nonetheless, the phenomenological models presented above contain a large number of adjustable parameters that need to be determined by fitting with experimental data. This limitation restricts the

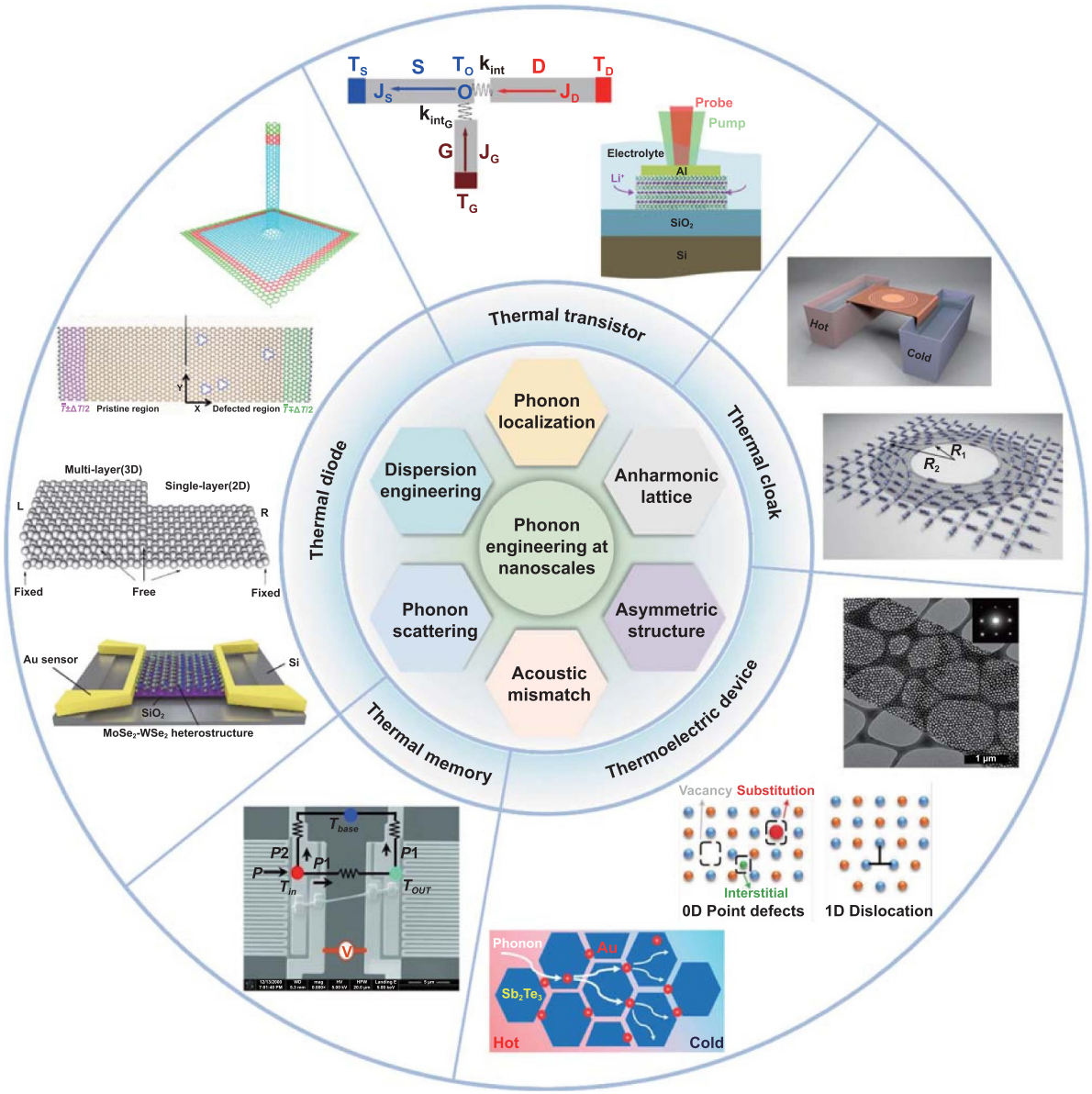

Figure 1. Schematic diagram of the strategies for phonon engineering and phononic devices at the nanoscale. Reprinted from [10], with the permission of AIP Publishing. Reprinted from [11], with the permission of AIP Publishing. Reprinted from [12], with the permission of AIP Publishing. Reprinted with permission from [13]. Copyright (2017) American Chemical Society. From [14]. Reprinted with permission from AAAS. Reproduced from [15], with permission from Springer Nature. [16] John Wiley & Sons. Copyright © 2011 WILEY-VCH Verlag GmbH & Co. KGaA, Weinheim. [17] John Wiley & Sons. © 2018 WILEY-VCH Verlag GmbH & Co. KGaA, Weinheim. Reprinted with permission from [18]. Copyright (2019) American Chemical Society. Reprinted with permission from [19]. Copyright (2010) American Chemical Society. Reprinted figure with permission from [20], Copyright (2013) by the American Physical Society.

prediction of thermal conductivity [25]. Besides, the relaxation time in the models is generally calculated from the relaxation times of diverse scattering sources according to Mattheissen's rule. The implicit assumption here is that different scattering types are independent of each other, but in fact they may interact and couple with each other. Therefore, detailed mechanisms of the thermal phonon transport processes remain to be further investigated.

In recent years, the development of computer science and measurements of thermal science has provided us with effective means to study the detailed scattering mechanisms inside microscopic heat carriers. Classical MD was first proposed by Alder and Wainwright [26] in 1959. They put forward a simulation method based on the hard sphere potential to study the behaviors of hundreds of classical particles interacting with each other. MD neglects the motions of electrons according to the Born–Oppenheimer approximation, and only takes the nuclei as the research objects. Empirical potential fields are used to describe the interactions between the nuclei and then deduce the trajectories of atoms or molecules based on Newtonian mechanics. Afterwards, the evolution of the system over time was observed, and the macroscopic physical and chemical properties of the system were obtained through statistical thermodynamics. Potential functions are very important

to the accuracy of simulation results, whereas the construction and selection of the potential functions require deep understanding of the material structures, bringing difficulties to the MD simulations. In 1985, Car and Parrinello [27] proposed a unified approach of MD and density functional theory (DFT). Under the Born–Oppenheimer approximation, classical MD of the atomic nuclei was combined with the electronic structure theory to solve Schrödinger equation, and then obtained almost all the ground-state properties of the material. This approach ushered in the era of first-principle simulations, which include *ab initio* and DFT. *Ab initio* is first-principle calculation in a narrow sense. In the calculation, various approximations such as single-electron approximation, non-relativistic approximation, and periodic potential field approximation are utilized. DFT is an advancement of the *ab initio* method, which calculates various properties of a particle system by replacing the wave function with the density distribution function of electrons as the only variable describing all the properties of the system. The aforementioned molecular simulation methods, namely MD [28], *ab initio* [29], DFT [30, 31] and the atomistic Green's function [32], are capable of performing high-fidelity simulations and predictions of thermal phenomena and thermal properties.

On the experimental side, advances in thermometry, such as the 3ω method [33, 34], T-type method [35, 36], H-type method [37, 38], Raman thermometry [39–46], time-domain and frequency-domain thermoreflectance (TDTR and FDTR) [4, 47–53], have enabled the characterization of heat transport processes and thermal properties on smaller spatial and temporal scales. Raman thermometry is a non-contact optical temperature measurement technology that utilizes Raman scattering. It is widely used for measuring thermal properties such as thermal conductivity, thermal diffusivity, and thermal contact resistance. Laser flash Raman spectroscopy method for characterizing transient thermal transport processes was first proposed by Li *et al* [41] in 2014. Compared to traditional steady-state methods, this method does not require the accurate value of the laser absorption coefficient and can also eliminate the influence of thermal contact resistance, which greatly improves the accuracy of measurements. In 2017, Yuan *et al* [42] developed energy transport state-resolved Raman (ET-Raman), which is capable of measuring interfacial ET and thermal carrier diffusion. The time resolution can reach the picosecond scale. In 2019, Fan *et al* [43] pointed out that dual-wavelength flash Raman method can be used for the characterization of anisotropic thermal properties. The emergence of tip-enhanced Raman scattering has significantly improved the spatial resolution of Raman thermometry [44, 45], allowing for measurements and imaging at sub-10 nm scales [47, 48]. This advanced technique can be utilized to explore ballistic thermal transport at nanoscale hotspots [48]. TDTR and FDTR are also non-contact measurement technologies for thermal properties, which measure the temperature change of nanomaterials through the change of surface reflectance of metal films on nanomaterials. In 1983, Eesley [52] first applied picosecond pulsed laser to the measurement of thermal physical properties, which served as the prelude to the development of TDTR. TDTR is a promising measurement method that is highly scalable. Through adjusting the elliptical ratio and size of the light spot, the in-plane thermal conductivity of two-dimensional materials in multiple directions can be simultaneously measured [53, 54], and thermal conductivity imaging at the micrometer-scale resolution can be realized [55–57]. In addition, TDTR can achieve high-precision measurement of thermal conductivity of thin films with substrates by utilizing laser signals of different frequencies [58]. As a variant of TDTR, FDTR replaces mechanical displacement by modulating the frequency of pump light, which leads to lower cost and higher precision. These measurement methods are powerful tools for scholars to pursue research, enabling them to gain a deeper understanding of phonon transport, and propose strategies for tuning thermal properties through phonon engineering.

Phonon scattering determines phonon transport behaviors. At different scales, phonons of various scattering types and different mean free paths (MFPs) contribute diversely to heat transport, leading to different modes of heat transfer and various strategies for phonon modulation. When the structural feature size L is much greater than the phonon MFP, three-phonon Umklapp scattering is dominant at high temperatures, and the heat transfer follows the classical thermal diffusion regime. At high temperatures, when there are only acoustic phonons participating in heat transport and Umklapp scattering dominates the other scattering processes, phonon thermal conductivity can be written as $k_L = A\frac{M\theta^3\delta}{\gamma^2 n^{2/3}T}$ [59], where M is the average mass of atoms in the crystal, θ is the Debye temperature, δ^3 is the volume of one atom, n is the number of atoms per original unit cell, and γ is the Grüneisen range. The Grüneisen parameter is derived from Grüneisen's law of thermal expansion [60], and measures the degree to which the lattice vibrational spectrum deviates from that of a purely harmonic crystal [61]. The higher the crystal anharmonicity, the larger the Grüneisen parameter and the lower the phonon thermal conductivity. Besides, it is also possible to change the phonon scattering characteristics or dispersion by introducing defects or isotopes inside the crystal or introducing interfaces and nanoparticles outside, thereby affecting the thermal transport characteristics of the crystal. The Zn_4Sb_3 prepared by Snyder *et al* [62] contained significant disorder, with zinc atoms distributed at the disordered interstitial sites, so the material exhibited an unusually low thermal conductivity. Biswas *et al* [63] incorporated SrTe nanocrystals in a PbTe matrix to form interfaces and defects, resulting in a 55% reduction in the thermal conductivity at ~800 K. Kargar *et al* [64] engineered the phonon spectrum of bulk crystals via introducing a small concentration of dopant atoms and found that even at extremely low concentrations of dopant atoms (~0.1%), phonon velocities were profoundly reduced.

When the structural feature size L is smaller than the MFP but much larger than the dominant phonon wavelength λ_0, the interfaces and boundaries will introduce size effects, where $\lambda_0 = 1.48\frac{V_S\hbar}{k_B T}$, k_B is the Boltzmann constant, T is the absolute temperature, and V_S is the sound velocity. For many crystalline materials, λ_0 is on the order of 1.5–2 nm at room temperature

[8]. The size effect is derived from the discovery that the crystal thermal conductivity is dependent on the sample size at low temperatures. Casimir interpreted this phenomenon as the boundary scattering of phonons. When the temperature is lower than a certain value, the MFP will increase to be comparable to the dimensions of the crystal, and the scattering of phonons at the crystal boundary will cause additional thermal resistance [65]. With the ever-decreasing size of devices and structures, Casimir size effect becomes more prominent at room temperature or higher, resulting in lower effective thermal conductivities than their parent bulk materials. For example, Li *et al* [66] observed that the thermal conductivity of single crystalline intrinsic silicon nanowires was more than two orders of magnitude lower than that of bulk silicon. Cheaito *et al* [67] reported that the thermal conductivities of nanoscale silicon–germanium alloy thin films were also much lower than the bulk values. Boundaries can also be combined with defects to scatter different spectral parts of phonons, further reducing thermal conductivities. Therefore, Casimir size effect of nanomaterials is of great interest in the field of thermoelectricity.

When the structural feature size L is much smaller than the MFP but slightly larger than λ_0, the spatial confinement of the phonon modes flattens the dispersion branches if the structure is freestanding or embedded in a material with different elastic properties, The population average phonon group velocity is reduced, leading to a dramatical increase in the phonon relaxation rates in defects and Umklapp processes [68]. The reduction of thermal conductivity is beneficial to the improvement of the performance of thermoelectric devices, but it makes thermal management of microelectronic devices a challenge. Later, scholars discovered that in thin films or nanowires embedded in 'acoustically fast' (higher sound velocity) or 'acoustically hard' (higher acoustic impedance) materials, the phonon group velocities and thermal conductivities could be enhanced along certain directions. Pokatilov *et al* [1] theoretically studied the influence of coatings made of different elastic materials on the acoustic phonon properties of semiconductor nanowires. It was observed that the phonon energy spectrum was compressed and phonon group velocities were greatly reduced when coated with a material with a low sound velocity, whereas when the surface was coated with a material with a high sound velocity, the phonon group velocities increased.

When the structural feature size L decreases to less than λ_0, phonon boundary scattering conceals intrinsic phonon scattering and dominates the heat transport process [69], and the ballistic transport mode becomes the dominant heat conduction mode [70]. In this ballistic regime, phonons can travel ballistically along straight trajectories for hundreds of nanometers. If the direction of motion of ballistic phonons can be controlled, thermal manipulation at this scale can be achieved. Anufriev *et al* [71] used silicon membranes with arrays of holes to control the direction of transmission of ballistic phonons. The results showed that aligned lattices dissipated heat faster than staggered lattices, and ballistic phonon transport exhibited a certain directionality in aligned lattices, which was enhanced with an increasing number of rows of holes and shrinking necks. Based on the above research, they illustrated possible applications of directional ballistic phonons in emitting heat rays, filtering heat flux and thermal shielding [72].

3. Phonon engineering at nanoscale

The development of nanotechnology has opened up new development opportunities and broad application prospects for phonon manipulation. Analogous to micro–nano electronic components, concepts and models of phonon devices (thermal diodes [73, 74], thermal transistors [10], thermal logic gates [75], and thermal memories [76]) have been proposed. Since signals encoded by heat outperform those encoded by electricity [8], thermophononic devices have the potential to revolutionize modern industry as much as microelectronics. Nanoscale phonon manipulation can assist in the design and realization of phononic devices. The following is a review of the research progress in the realization and enhancement of thermal functional applications such as thermal rectification, phonon information processing, and thermoelectric conversion through phonon modulation at the nanoscale.

3.1. Thermal rectification (thermal diode)

Thermal diodes can realize active regulation of heat flux. Applying a positive thermal bias causes the thermal diode to behave as a good conductor of heat, while a negative thermal bias causes it approximately a thermal insulator. The thermal rectification ratio (TR) is a key parameter for evaluating thermal diodes. It is generally defined as the ratio of the difference between the forward and reverse thermal conductance and the weaker reverse thermal conductance. In specific calculations, physical quantities such as heat flow and thermal conductivity are usually used to characterize thermal conductance.

The initial experimental observation of thermal rectification can be traced back to Starr's study of the interfacial characteristics of copper/cuprous oxide in 1936 [77]. It was observed in the experiment that the thermal conductivity was higher in the direction of higher electrical conductivity. In such metal/insulator systems, the two materials primarily transmit heat to each other through two different types of carriers, electrons and phonons, so there must be electron–phonon scattering at the interface for energy exchange. Due to the energy-dependent scattering rate, the energy transferred from phonons to electrons will differ from that transferred from electrons to phonons, resulting in thermal rectification [78]. In composites composed of different metals, thermal rectification phenomena have also been observed due to asymmetric transport of carriers at interfaces [79, 80]. This asymmetry originates from the difference in the work function of the materials on the two sides of the interface. When the material with a higher work function is at high temperature, fewer electrons will be excited, and the potential barrier at the interface will hinder the migration of electrons, leading to lower heat conduction than that in the opposite direction. Different temperature dependence of thermal conductivity of the two materials constituting the interface [81–83] and thermal strain/warpage at interfaces

[84, 85] also contribute to thermal rectification phenomena in bulk materials.

However, the unique heat transport characteristics of nanomaterials enable them to have potential mechanisms for thermal rectification that are different from those of macroscopic materials [86], including matching/mismatching of phonon spectra, phonon localization, asymmetric phonon scattering and temperature dependence of thermal conductivity, which are inherently interrelated and influenced by each other. The best way to achieve thermal rectification at nanoscales is to exploit the nonlinear dynamics present in anharmonic lattice structures in combination with the inherent asymmetric structure of the system [8]. Specifically, asymmetric structures can be roughly classified [87] into asymmetric geometry [11, 37, 88–91], asymmetric doping and defects structures [12, 92, 93], asymmetric interfacial structures [13, 14, 94, 95], and other structures [96–98].

3.1.1. Asymmetric geometry. Constructing an asymmetric geometric structure is the most basic and simplest way to realize thermal rectification. Due to its proved superior thermal conductivity, graphene is likely to become the promising candidate material for nanoscale thermal management in the future, so it has also become one of the major research objects in the field of thermal rectification. Hu *et al* [28, 88] studied the thermal rectification of monolayer and bilayer triangular and trapezoidal graphene nanoribbons (GNRs) based on classical MD simulations, and discussed the size dependence of the rectification effect. The results showed that the heat flow preferentially propagated in the direction of decreasing width. Figure 2(a) shows the TR versus temperature for monolayer rectangular, monolayer triangular, monolayer trapezoidal, and double-layer triangular GNRs, among which the single-layer triangular GNRs has the highest TR, reaching 120% at 180 K.

Graphene Y junctions also exhibited an obvious thermal rectification effect, which was caused by match/mismatch the phonon DOS spectra between the two ends [89]. When the temperature of the branch end is higher than that of the stem end, the phonon power spectra at both ends overlap in a larger frequency range, facilitating the passage of phonons through the graphene Y junction. Conversely, when the temperature of the branch end is lower than that of the stem end, an obvious mismatch in the power spectra occurs, thereby impeding the transport of phonons through the structure. What's more, compared with the monolayer graphene Y junctions, the simulation results of the double-layer structures showed a larger TR. In the double-layer GNR, the stronger nonlinearity is induced by the layer–layer interaction, and the nonlinearity has been shown to favor thermal rectification [96].

In experiments, target-shaped asymmetric GNRs can be fabricated by photolithography, such as extreme ultra-violet lithography and electron beam lithography, and the thermal rectification effects can be measured using microelectrodes. Wang *et al* [37] designed three suspended monolayer graphene devices with different asymmetric nanostructures and studied their thermal rectification behaviors. The first was graphene with nanopores on one side, as shown in samples #1, #2, and #3 in figure 2(f). The thermal conductivity from the nanopore area to the non-porous area was prominently higher than that in the opposite direction, and the average TR was about 26%. The authors identified the underlying cause of thermal rectification in the asymmetric defect-engineered samples was the dependence of thermal conductivity on temperature and location. As for the second device, nanoparticles were deposited on one side, as shown in sample #4 in figure 2(f). After the nanoparticles were deposited by electron beam induction, the heat flux was 10% higher from the clean region to the nanoparticle deposition region than that in the opposite direction. The third was graphene with a tapered width, as shown in sample #5 in figure 2(f). The measured thermal conductivity was 11% higher when heat flowed from the wide side to the narrow side. Asymmetric phonon scattering is the physical mechanism that produces thermal rectification in the second and third structures. The presence of nanoparticles induces significant additional phonon scattering such that fewer phonons propagating modes can reach the cold side. Similarly, the trapezoidal graphene exhibits additional phonon scattering due to the stronger edge scattering effect at its narrow end.

MoS_2 spontaneously grows to form a very regular triangular structure with natural asymmetry, which is very suitable for the fabrication of nanoscale thermal rectifiers. Yang *et al* [90] discovered that the TR of the monolayer MoS_2 sample could reach up to around 70%, and increasing the vertex angles of samples and the space between sensing electrodes would raise the TRs. Silicon films can also be used in the manufacture of thermal diodes. Kasprzak *et al* [91] prepared silicon membranes with asymmetric porosity as thermal rectifiers, achieving a TR of about 14%. At the hot ends, phonon–phonon scattering dominates other scattering processes and the porosity has a subordinate effect on the MFPs, while at the cold ends, boundary scattering near the holes is dominant, and high porosity will greatly shorten the MFPs of phonons, which causes a rapid decrease in the thermal conductivity. As a result, the apparent thermal conductivity is higher when the region with high porosity is the hot end.

Thermal rectification in 3D structures is also worthy of investigation. Zhong *et al* [11] studied thermal rectification in thickness-asymmetric GNRs which was comprised of multilayer graphene in one segment and monolayer graphene in the other segment. As shown in figure 2(e), when phonons transmit from the monolayer to multilayer, that is, from a 2D structure to a 3D structure, they have more channels to pass through smoothly. Instead, the phonons that go from multilayer to monolayer must smash apart near the junction where the 3D structure connects to the 2D structure. An increase in the average temperature leads to a fall in the TR due to the fact that the phonon scattering of monolayer graphene increases steadily with the increasing temperature, and when the temperature rises to the point where the Umklapp scattering in monolayer graphene approaches that in the junction, the TR tends to be zero.

In summary, higher asymmetry signifies greater thermal rectification ratio. Asymmetric geometric structures are mainly achieved via the asymmetric geometric shapes in the plane, such as rectangles, trapezoids, triangles, etc. In the

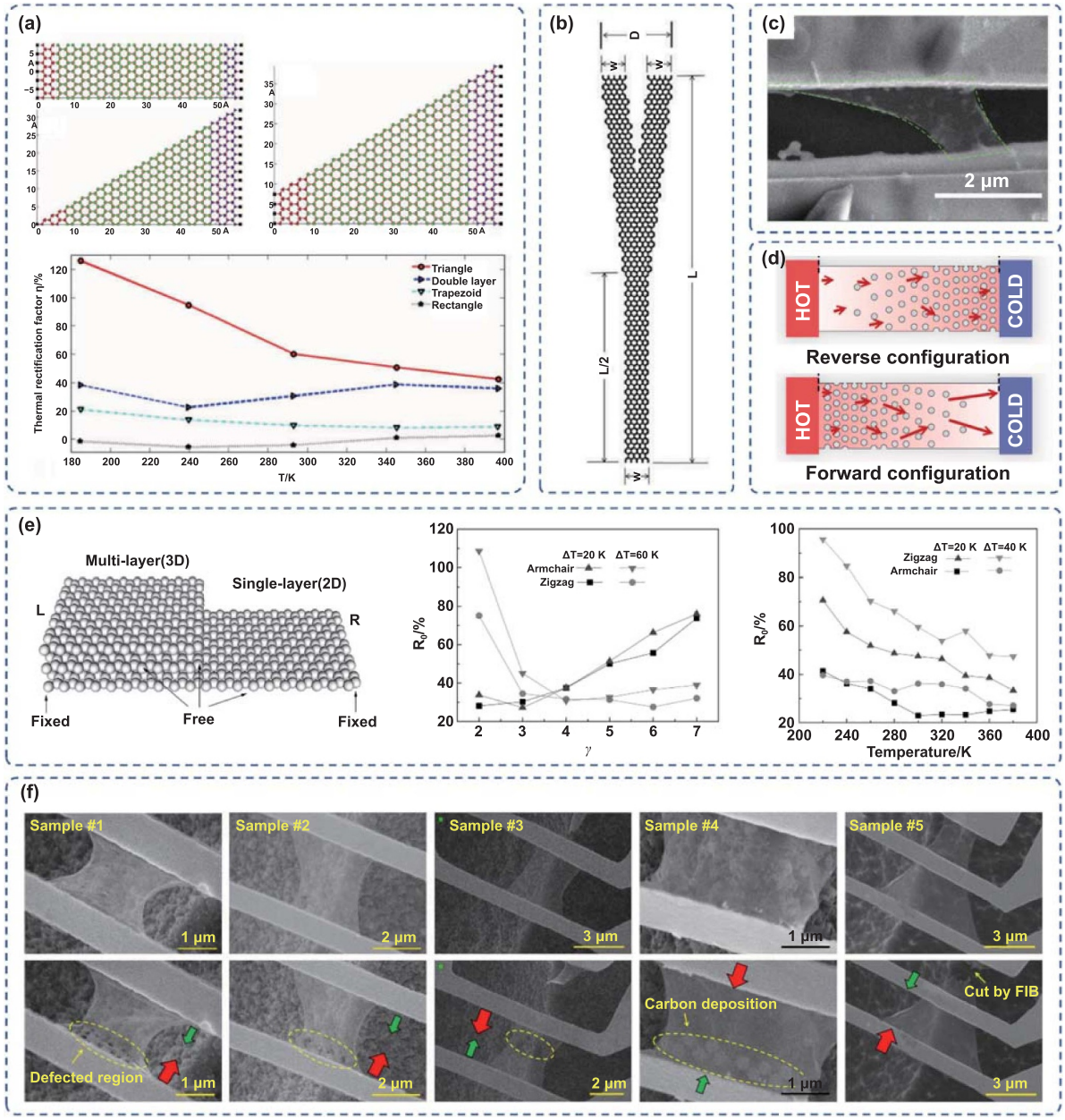

Figure 2. Thermal rectifiers based on asymmetric geometric structures. (a) Rectangle, triangle and trapezoid GNRs. Reproduced from [88], with permission from Springer Nature. (b) Graphene Y junction. Reproduced from [89] with permission from the Royal Society of Chemistry. (c) Scanning electron microscope (SEM) image of the MoS_2 sample. Reprinted with permission from [90]. Copyright (2020) American Chemical Society. (d) Silicon membranes with asymmetric porosity. Reprinted from [91], Copyright (2020), with permission from Elsevier. (e) Thickness-asymmetric GNR. Reprinted from [11], with the permission of AIP Publishing. (f) SEM images of the suspended monolayer graphene devices. Several nanopores were drilled in samples #1, #2 and #3. Sample #4 is graphene with asymmetric carbon deposition. Sample #5 is graphene with a tapered width. Reproduced from [37], with permission from Springer Nature.

future, more complex shapes should be attempted. According to the current state of the art, this can be realized in both simulations and experiments. In the study of the dependence of the rectification effect on the number of nanoribbon layers, different literatures have given different results. For instance, the TR of bilayer graphene Y junctions is higher than that of monolayer Y junctions, while the TR of double-layer triangular GNRs is lower than that of single layer triangular GNR. This may be attributed to the different transport characteristics of phonons and mechanisms of thermal rectification in different structures.

3.1.2. Asymmetric doping and defects structures. Doping and defects can also act as structural asymmetries to achieve thermal rectification. The mismatch of phonon power spectra caused by doping and defects is a crucial mechanism for thermal rectification. The phenomenon of thermal rectification

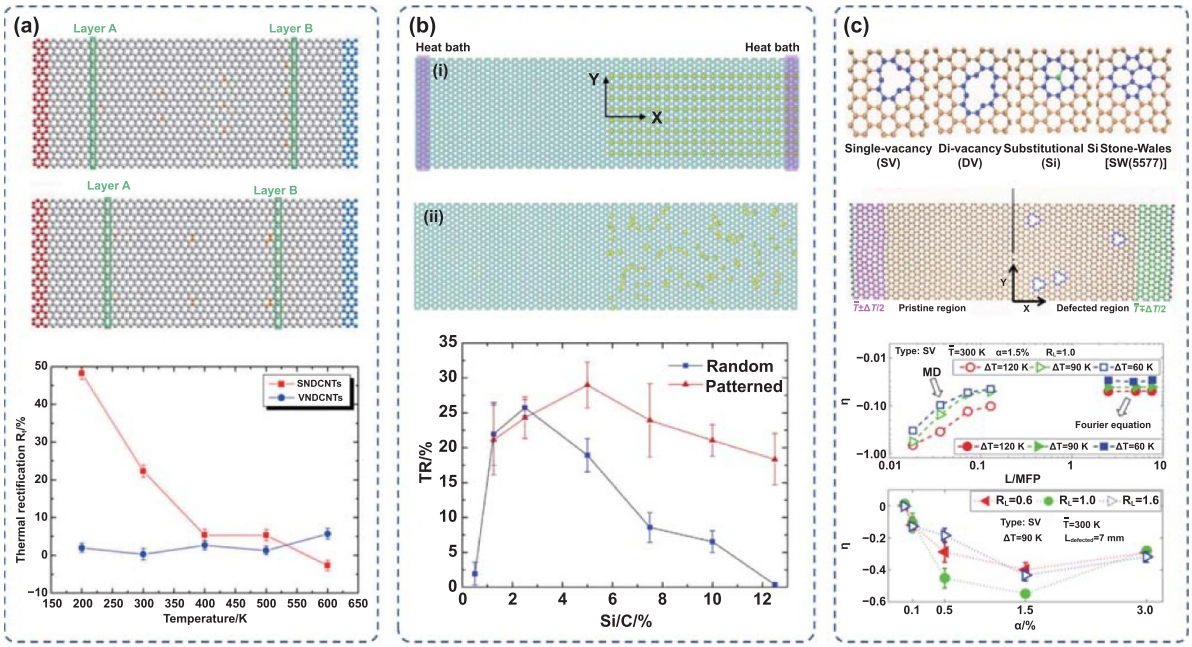

Figure 3. Thermal rectifiers based on asymmetric doping or defects. (a) Triangular single-nitrogen-doped graphene and parallel various-nitrogen-doped graphene. Reprinted from [92], Copyright (2010), with permission from Elsevier. (b) Silicon-functionalized GNRs with patterned distribution and random distribution. Reprinted from [93], Copyright (2015), with permission from Elsevier. (c) Types of point defects studied by Wang *et al* [12]. Reprinted from [12], with the permission of AIP Publishing.

in carbon nanotubes (CNTs) with geometric variations of doped nitrogen was investigated by Chien *et al* [92]. The rectification effect of the triangular single-nitrogen-doped CNTs (SNDCNTs) was better than that of the parallel various-nitrogen-doped CNTs (VNDCNTs). At 200 K, SNDCNTs had the largest TR (48.2%). Calculations of the phonon power spectra revealed the reason. When the heat flux transports from left to right in SNDCNTs, the phonon power spectra of the A and B layers are well matched, which is beneficial to phonon transport. In the opposite direction, the matching degree of phonon power spectra is low, which makes it hard for phonons to transport from left to right. VNDCNTs have similar overlapping areas in both directions, and thus have little rectification effect.

Yuan *et al* [93] explored thermal rectification in silicon-functionalized GNRs, and discovered that the TR could be tailored by adjusting the functionalization distribution and ratio. As the Si/C ratio increased from 0.5% to 12.5%, the thermal rectification ratio initially increased before decreasing by degrees. So there exists an optimal functionalization ratio. The optimal ratio is about 2.5% for randomly functionalized GNRs and about 5% for GNRs with ordered arrangement of silicon atoms. At high Si/C ratios, the TR of randomly functionalized GNRs is lower than that of regularly functionalized GNRs, which is due to stronger phonon localization and lower group velocities caused by randomization.

Using non-equilibrium MD, Wang *et al* [12] revealed the influence of four different defect forms (SV, DV, Si and SW, figure 3(c)) and different defect concentrations on the rectification effect on GNRs. Under the same defect concentration, SV and Si defects would make graphene obtain more dispersed defect nodes, hence obtaining a better TR than DV and SW defects. It was found that the TR of 1% defect concentration was the highest. The 14 nm long and 4 nm wide GNRs could achieve a TR of up to about 80% at an ambient temperature of 200 K and a bias temperature of 90 K. By adjusting the length of GNRs, it was found that the TR dropped with increasing length, and eventually stabilized at a length-independent value of roughly 3%–5% (figure 3(c)).

Type, concentration and distribution of dopants and defects are crucial factors affecting the rectification effect. The greater the difference in mass between dopant atoms and original atoms is, the stronger the asymmetric phonon scattering will be, resulting in a larger thermal rectification ratio. Both doping and defects have optimal concentrations. A low defect concentration will marginally alter the heat transport characteristics, while an excessively high defect concentration will drastically limit heat conduction and thermal rectification effect generated by asymmetric scattering. Doping and defects are suggested to be concentrated in a certain area of the material with ordered or asymmetric distributions. However, under the existing experimental conditions, it is difficult to achieve patterned and refined distributions [99], so further development of related technologies is necessary to support the implementation of this manipulation strategy.

3.1.3. Asymmetric interfacial structures. Connecting two different materials together to form a heterojunction, a thermal rectification effect will appear. Chen *et al* [94] reported the results of thermal rectification simulations of carbon/boron nitride heteronanotubes (CBNNTs). Heat preferentially flows from the BNNTs to the CNTs, and the TR of CBNNTs with a

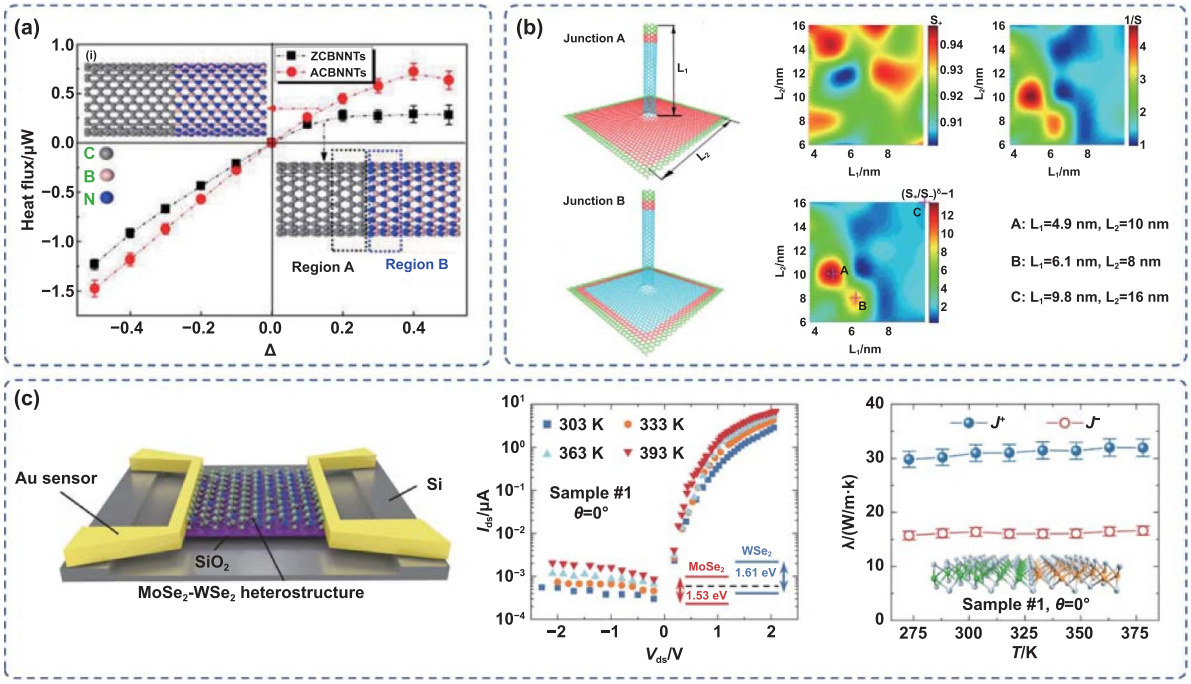

Figure 4. Thermal rectifiers based on heterojunctions. (a) Carbon/boron nitride heteronanotubes. Reprinted from [94], Copyright (2019), with permission from Elsevier. (b) SWCNT–graphene junctions. Reprinted with permission from [13]. Copyright (2017) American Chemical Society. (c) $MoSe_2$–WSe_2 lateral heterogeneous rectifier. Reprinted with permission from [14]. Copyright 2022 the authors, some rights reserved; exclusive licensee American Association for the Advancement of Science. From [14]. Reprinted with permission from AAAS.

length of 9.6 nm can reach 483%. The analysis of the transverse and longitudinal phonon power spectra revealed that the matching/mismatching of the low-frequency transverse phonon vibration modes was the primary mechanism causing thermal rectification. For better TRs, the length of the nanotubes is preferable to not exceed 10 nm and defects should be avoided as much as possible. As the tube length increases, the exciting kinetic energy waves become more difficult, and the increase in long-wavelength phonons makes it easier to transport heat across the interface. The presence of defects amplifies phonon scattering and weakens the asymmetry level of phonon scattering. Their research team also measured the TR of the graphene/hexagonal boron nitride heterojunction, up to 286.1% [95]. They attributed this to a mismatch of out-of-plane phonons modes.

Yang *et al* [13] found the maximum TR of the SWCNT-graphene junction could reach 1681.6% at the average temperature of 200 K, far greater than the reported values of thermal rectifiers based on single-material nanostructures. The TRs of nanotube-graphene junctions were quite sensitive to geometry size. Through calculating the overlap degree of phonon power spectra (figure 4(b)), the authors found that the degree of overlap of phonon spectra under positive thermal bias (S_+) was not sensitive to geometry size, while the degree under negative thermal bias (S_-) was fairly sensitive to geometry size, and the trend was similar to that of the TR. Aside from the asymmetric interface, the asymmetric thermal contact at the boundary is also the primary cause for the ultrahigh thermal rectification, and its effect is even more prominent than that of the asymmetric interface.

In 2022, Zhang *et al* [14] successfully developed the first two-dimensional lateral heterogeneous integrated electrical and thermal rectifier (figure 4(c)). The phonon spectra showed that when the heat flowed in the direction from $MoSe_2$ to WSe_2, the overlap of phonon spectra was substantially higher than that in the reverse way. At the same time, the exchange between Mo and W atoms as well as the narrow edges at the interface brought about by the zigzag structure led to more localized phonon modes from WSe_2 to $MoSe_2$ direction, further enhancing the thermal rectification. The combined effects of these two mechanisms resulted in a TR of up to 96% and a high electrical rectification ratio of 10^4 at the atomically thick two-dimensional heterojunction. It was found that the rectification effect was dependent on the angle between the heterojunction interface and heat flow direction. When electrons and phonons passed vertically through the heterojunction interface, the device had the highest rectification ratio, while when the transport direction was parallel to the interface, the rectification effect disappeared. Furthermore, the research group found that the thermal rectification effect would significantly improve the heat dissipation capability of electronic devices under high power conditions. When the diode is in the positive state, the current through the device increases rapidly with the increase of power, and an obvious temperature gradient is formed from $MoSe_2$ to WSe_2 direction, which is exactly the preferred direction for phonon transport in heterojunction

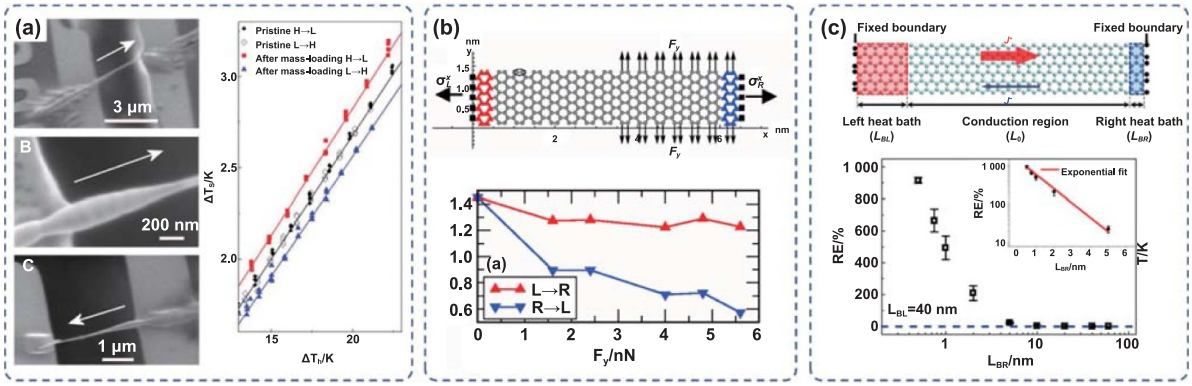

Figure 5. Thermal rectification realized by applying asymmetric mass loading, asymmetric stress fields, and asymmetric thermal contact. (a) SEM images of BNNTs after deposition of $C_9H_{16}Pt$. From [96]. Reprinted with permission from AAAS. (b) Rectangular GNR under non-uniform strain fields. Reprinted figure with permission from [97], Copyright (2012) by the American Physical Society. (c) Pristine monolayer graphene with asymmetric thermal contact. Reprinted from [98], with the permission of AIP Publishing.

diodes, thus promoting the thermal conductivity in this direction by 96%. The increase in the thermal conductivity of the material will tremendously improve the heat dissipation performance of the device. The experimental results demonstrated that under a large bias voltage of 60 V, the local temperature rise of the monolayer 2D heterojunction rectifier was about 20% lower than that without thermal rectification effect.

The constituent materials of heterojunction structures can be freely selected. Owing to the difference in the phonon spectra of the materials on both sides, heterojunctions exhibit stronger thermal rectification abilities, and the rectification ratios are typically one to two orders of magnitude higher than that of thermal rectifiers based on single-material nanostructures. Two different materials can not only form lateral heterojunction, but also normal heterogeneous rectifier, providing a new direction for the development of smaller thermal diodes. Besides, the interface geometry and the angle between the heat flow direction and the interface can be changed to adjust the rectification effect and realize directional rectification. It should be noted that defects should be avoided as much as possible during the preparation of heterojunction thermal rectifier devices, since many literatures [100, 101] have revealed that defects would reduce the thermal rectification ratio.

3.1.4. Other structures. Thermal rectification can also occur under the existence of asymmetric mass loading. Chang *et al* [96] modified CNTs and boron nitride nanotubes (BNNTs) by amorphous $C_9H_{16}Pt$ particles loading externally and inhomogeneously. The resulting asymmetric axial thermal conductance yielded a TR of 2% for CNTs and 7% for BNNTs (figure 5(a)). The direct thermal contribution of $C_9H_{16}Pt$ has been proved to be negligible. The authors suggested that the nonperturbative solutions of nonlinear systems, that is, solitons may be responsible for thermal rectification. Solitons are localized particle-like entities that can collide with each other yet retain their shapes. In general, soliton models exhibit an asymmetry in heat transport for inhomogeneous media [102, 103]. Due to the enhanced nonlinearity caused by the stronger ionic nature, BNNTs exhibited a greater thermal rectification effect than CNTs.

Stress and strain can alter characteristic vibration frequencies and lattice anharmonicity, hence affecting thermal transport. Different stresses result in different changes, and the ensuing asymmetry of vibration characteristics induces a local variation of thermal conductivity. This change, combined with temperature dependence of thermal conductivity, enables phenomena of thermal rectification. Gunawardana *et al* [97] investigated thermal rectification properties in rectangular GNRs subject to non-uniform stress fields. Using MD simulations, the research group observed that the heat flux from the less stressed zone to the more stressed zone was larger than that in the reverse way. The forward heat flow had little attenuation with increasing stress, whereas the reverse heat flow was remarkably reduced (figure 5(b)). The maximum TR exceeded 70%.

Setting asymmetric thermal contact is a novel method to achieve thermal rectification in materials without asymmetric structures. Jiang *et al* [98] adopted this strategy in pristine monolayer graphene. About 920% TR was achieved in 200 nm long samples, and about 110% TR in samples at a micrometer scale. The simulation results demonstrated that the TR decreased exponentially with the increase of the length of the right heat bath L_{BR} (figure 5(c)). When L_{BR} was short, for instance $L_{BR} = 0.5$ nm, the TR could reach as high as 920%. But when L_{BR} was longer than 5 nm, the thermal rectification phenomenon vanished. The analysis of the phonon participation ratio provided reliable evidence that the key is the localization length. When the length of thermal contact is shorter than the localization length, it will induce strong localization of low-frequency phonons, resulting in a remarkable temperature jump at the short thermal contact, and thus giving rise to notable TRs in symmetric pristine monolayer graphene. It should be noted that the length of the long thermal contact ought to be longer than the localization length to ensure the occurrence of thermal rectification effect.

Applying mass gradients, stress gradients, etc can achieve thermal rectification via modifying the anharmonicity of the lattice or the characteristic vibration frequencies. However, an

Table 1. Summary of the reported thermal rectification ratios in different studies.

Approach	Materials	TR	Physical mechanisms[a]	ΔT (K)	Authors	Time	Method
Asymmetric geometry	Thickness-asymmetric graphene	∼170%	3, 4	80	Zhong *et al* [11]	2011	Simulation
	Monolayer triangular graphene	120%	3	18	Hu *et al* [88]	2012	Simulation
	Graphene Y junctions	63%	1	120	Zhang and Zhang [89]	2011	Simulation
	Suspended monolayer MoS_2	70%		∼20	Yang *et al* [90]	2020	Experiment
	Graphene with defects on one side	26%	3, 4		Wang *et al* [37]	2017	Experiment
	Holey silicon	14%	3		Kasprzak *et al* [91]	2020	Experiment
Asymmetric doping and defects structures	Silicon-functionalized graphene	145%	2	150	Yuan *et al* [93]	2015	Simulation
	Asymmetrically defected graphene	80%	1	45	Wang *et al* [12]	2012	Simulation
	Triangular single-nitrogen-doped carbon nanotubes	48.2%	1		Chien *et al* [92]	2010	Simulation
Asymmetric interfacial structures	Single-carbon nanotube–graphene	1681.6%	1	100	Yang *et al* [13]	2017	Simulation
	Carbon/boron nitride heteronanotubes	483%	1	150	Chen *et al* [94]	2019	Simulation
	Monolayer $MoSe_2$–WSe_2	98%	1		Zhang *et al* [14]	2022	Experiment
Other structures	Graphene	920%		20	Jiang *et al* [98]	2020	Simulation
	Strained graphene nanoribbons	>70%		90	Gunawardana *et al* [97]	2012	Simulation
	Boron nitride nanotubes	7%			Chang *et al* [96]	2006	Experiment

[a] Physical mechanisms:
1. Matching/mismatching of phonon power spectra.
2. Phonon localization.
3. Asymmetric phonon scattering.
4. Temperature dependence of thermal conductivity.

increase in stress and strain often results in a drop in materials' thermal conductivities, making stress strategies less effective for materials with inherently low thermal conductivity. Compared with the modification of materials and complex structural design, applying external physical fields is a simpler way, which can adjust the thermal performance according to the application scenarios. Apart from the asymmetric mass field, stress field and temperature field, it is also possible to attempt to manipulate phonon transport through magnetic fields, electric fields, etc in the future.

3.1.5. Summary. In the current works on nanoscale thermal diodes, the physical mechanisms of the phonon manipulation methods for thermal rectification can basically be classified into the following four types: (1) matching/mismatching of phonon power spectra. If the power spectrum of one segment of the device matches its neighbors, heat can be exchanged efficiently. Without this overlapping spectral characteristic, the energy exchange is largely suppressed. Since the phonon power spectra are strongly dependent on temperature, it will achieve a smoother energy exchange if the temperature deviation induces the phonon spectra of different segments to overlap each other. However, strong heat transfer inhibition occurs if the phonon spectra of the different parts cannot overlap significantly for the opposite temperature deviation. This can explain the thermal rectification effect that occurs in many heterostructures and geometrically asymmetric structures. (2) Phonon localization. Anderson proposed the concept of electron localization in 1958 [104], pointing out that if impurities are added to the ordered lattice to generate disorder, electrons will be scattered by these impurities, and multiple scattered waves interfere with each other, which may cause the electrons to transform from the diffusion state to the localized state, that is, the movement stops. The electrons in the localized state do not contribute to the electrical conduction, and with the increase of the degree of disorder, the system may even change from a metal type to an insulator. Similar to electron localization, phonons in the localized state are almost unable to transfer heat, and the thermal resistance of this part is quite large macroscopically. Luckyanova *et al* [105] noted that due to multiple scattering and interference events of broadband phonons, superlattices embedded with nanodots at the interfaces exhibited notable phonon localization behaviors

in a broad frequency range, lowering thermal conductivities by over a factor of two. Therefore, inducing one-way phonon localization is one of the ways to induce thermal rectification. (3) Asymmetric phonon scattering. In [37], the presence of nanoparticles caused significant additional phonon scattering, so the heat flow was tremendously reduced when the nanoparticle deposition region was at high temperatures. For trapezoidal GNRs, the stronger edge scattering effect at the narrow end also made the heat flow smaller when a high temperature bath was applied to the narrow end than in the opposite direction. It is clear that one of the primary contributory factors of thermal rectification is the asymmetric scattering of phonons. (4) Temperature dependence of thermal conductivity. In [37], the thermal conductivity of pristine graphene was high and declined with rising temperature, while the thermal conductivity of graphene with nanopore defects was low and almost independent of temperature. Therefore, as a result of the substantial decline in the thermal conductivity of pristine graphene, the absolute value of the overall thermal conductivity reduction when a high-temperature thermal bath is applied to pristine graphene is greater than the thermal conductivity when a low-temperature thermal bath is applied to pristine graphene. In this case, thermal rectification occurs. Table 1 summarizes the maximum thermal rectification ratio values and their physical mechanisms in some reported literature.

In most studies, thermal rectifiers based on nanomaterials exhibit the common characteristic that the TR decreases with the increase of the average temperature and size of the system. Elevated temperature increases the total number of phonons, so that more phonons participate in heat transfer process, and at the same time enhances the Umklapp scattering, which gradually overshadows the asymmetric phonon scattering and dominates the heat transfer process, resulting in the weakening of the thermal rectification effect. Reduction of asymmetry and more excited long-wavelength phonons are the key reasons for the decrease of thermal rectification coefficient with increasing length. However, the above rules do not apply to all nanoscale thermal rectifier devices, as their thermal characteristics largely depend on the types and structures of their constituent materials. Among all the manipulation strategies of thermal rectifiers, heterojunctions have more advantages in realizing ultra-high TR due to their extremely high degree of asymmetry. In simulations, a rectification ratio of more than 2000% has been achieved. Due to the challenges in preparation of nanomaterials, the current rectification ratios are far lower than anticipated, but it indeed poses as a promising direction for future research.

3.2. Thermal transistor

The theoretical model of thermal transistors was initially proposed by Li *et al* in 2006 [10]. Like an electrical transistor that controls current, a thermal transistor is made up of three parts: a source (S), a drain (D) and a gate (G). When a constant temperature bias is applied between S and D, heat flux between S and D can be adjusted by the temperature applied to the gate. Most crucially, due to the transistor's ability to amplify the signals through the gate, a change in heat flow from the gate is capable of inducing a larger change in heat flow from S to D. The specific configuration of the model is shown in figure 6(a). As illustrated in figure 6(a), the system can be turned into a good conductor or insulator of heat by controlling the temperature T_{G}, and the heat flow ratio between the 'ON' and 'OFF' states is about 100. In order to examine the modulation and amplification functions of the transistor, differential thermal resistance R_{S} and R_{D}, and heat flow amplification coefficient α are defined as follows

$$R_{\mathrm{S}} = \left(\frac{\partial J_{\mathrm{S}}}{\partial T_{\mathrm{O}}}\right)^{-1}_{T_{\mathrm{S}}=\mathrm{const}} \tag{1}$$

$$R_{\mathrm{D}} = -\left(\frac{\partial J_{\mathrm{D}}}{\partial T_{\mathrm{O}}}\right)^{-1}_{T_{\mathrm{D}}=\mathrm{const}} \tag{2}$$

$$\alpha = \left|\frac{\partial J_{\mathrm{D}}}{\partial J_{\mathrm{G}}}\right| = \left|\frac{R_{\mathrm{S}}}{R_{\mathrm{S}}+R_{\mathrm{D}}}\right| \tag{3}$$

To get the amplification effect, α must be greater than 1, which means that either R_{S} or R_{D} must be negative, that is, negative differential thermal resistance (NDTR). In other words, a transport regime in which the heat flux decreases with increasing temperature gradient is desired. It is worth noting that NDTR is not absolute negative thermal resistance, and it does not conflict with any physical law.

As a crucial prerequisite for thermal transistors, phenomena of NDTR have recently been investigated in various systems. One way to achieve NDTR is to utilize materials whose thermal conductivity decreases significantly with increasing temperature. Hu *et al* [106] studied the nonlinear heat transport process in GNRs under large temperature biases. During the simulation, the temperature of the hot thermostat was kept as a constant, and the temperature bias was changed by reducing the temperature of the cold thermostat. When the temperature bias reaches a certain critical value, the heat flow decreases when the temperature bias increases, indicating that the phenomenon of NDTR occurs. When the thermal conductivity is constant, an increase of the temperature bias tends to increase the heat flux. However, the increase of the temperature bias means that the average temperature of the GNR drops, giving rise to a drop of the average thermal conductivity and a reduction of heat flow. The reduction effect of the latter offsets the gain effect of the former, so the NDTR appears.

Compared with single materials, heterojunction interfaces have been found to demonstrate a good reflection effect on the low-frequency transverse sound wave under large temperature differences, which can be leveraged to create an NDTR. Chen *et al* [95] investigated NDTR behaviors of graphene/hexagonal boron nitride heterojunctions. It was observed that when the temperature bias was large enough, the transverse acoustic wave was excited in the boron nitride domain, which would be reflected back at the interface, making it difficult to transfer heat from boron nitride to graphene. Therefore, the heat flow decreased and the phenomenon of NDTR appeared.

The core of NDTR lies in thermal conductivity reduction of materials under large temperature differences. In addition

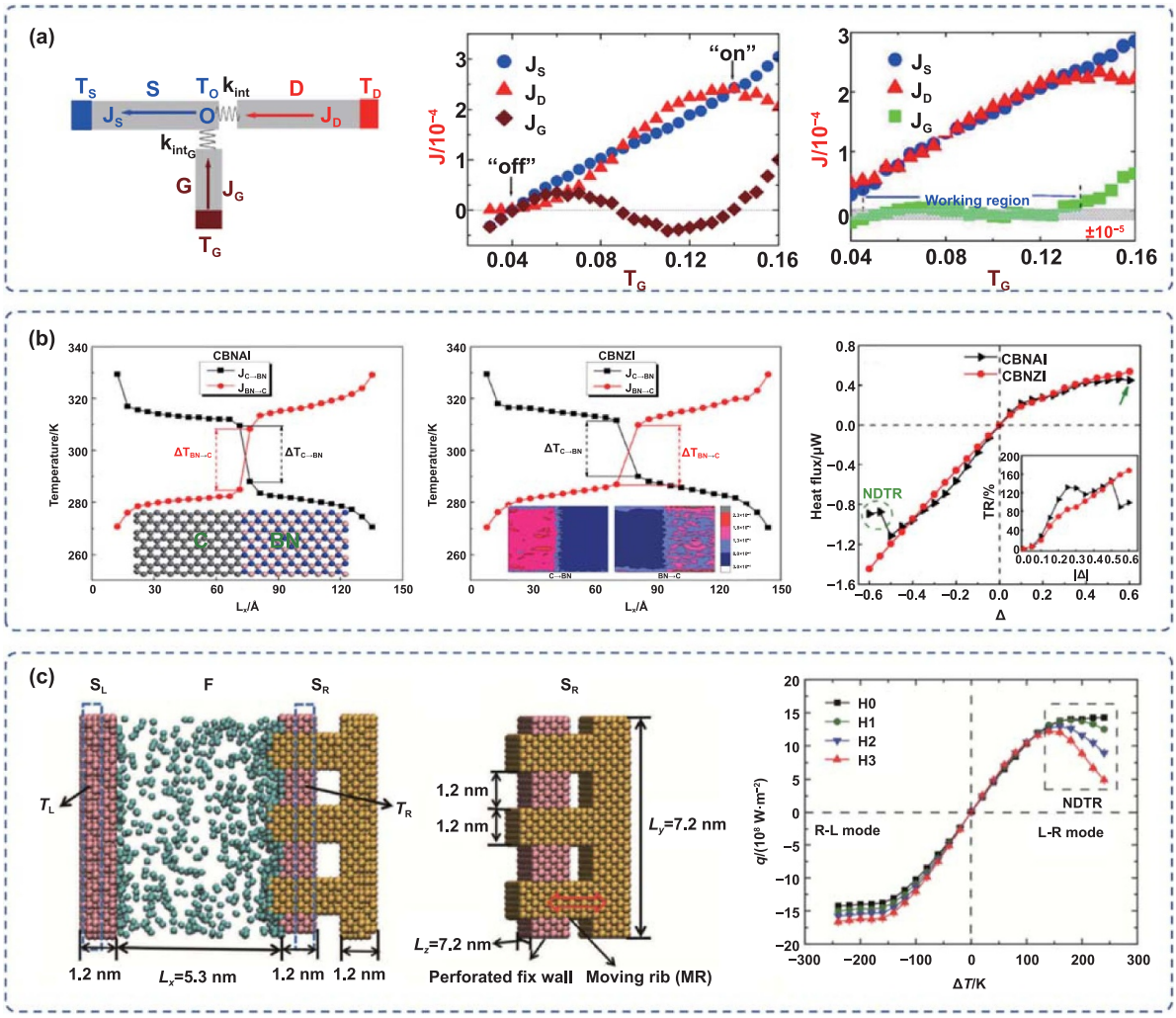

Figure 6. A theoretical model of thermal transistors, and NDTR behaviors in various systems. (a) Theoretical model of thermal transistors. Reprinted from [10], with the permission of AIP Publishing. (b) Graphene/hexagonal boron nitride heterojunction. Reprinted from [95], Copyright (2016), with permission from Elsevier. (c) Gas-filled nanogap with movable rib (MR, yellow) in one side. Reproduced from [107], with permission from Springer Nature.

to utilizing the characteristics of solid materials, NDTR can also be realized by leveraging the low-temperature adsorption characteristics of fluid molecules. Li *et al* [107] designed a gas-filled nanostructure with mechanically-controllable nanopillars, as shown in figure 6(c). The movable rib can be inserted into or removed from the nanogap to control the height of the MR. The NDTR phenomenon (figure 6(c)), which was brought on by fluid adsorption on the cold solid surface, occurred when the temperature difference (ΔT) between the two sides exceeded 140 K. In the case of a high-temperature heat bath with a fixed temperature applied on the left solid, the rise of ΔT means the drop of the temperature T_{R}, and a large number of fluid molecules adsorbed on the cold solid surface, resulting in the decrease of free fluid molecules, and the decrease of thermal conductivity in the nanogap. This not only counteracts the effect of increasing temperature gradients, but also leads to a reduction in heat flow. Controlling the height of nanopillars could substantially enhance the NDTR effect.

In recent years, many researchers have achieved functionality of thermal transistors through theoretical models or experiments. Graphene is a potential candidate material for thermal transistors according to calculations demonstrating the NDTR phenomenon. Zhong *et al* [108] investigated the thermal control in three-terminal GNRs (figure 7(a)) using MD simulations. As shown in figure 7(a), the GNRs behaved as a poor thermal conductor at a low gating temperature of $T_{\mathrm{G}} \sim 10\,\mathrm{K}$ and this is the 'OFF' state, while at $T_{\mathrm{G}} = 224\,\mathrm{K}$, the heat flow was enlarged about 20 times compared to the 'OFF' state, and this is the 'ON' state. This structure can also be used to amplify the input thermal signal. Define the amplification efficiency as the ratio of the output temperature change to the input temperature change as $G_0 = \frac{\Delta T_{\mathrm{out}}}{\Delta T_{\mathrm{in}}}$. At extremely low input temperatures, the amplification efficiency could reach a maximum of 3.2. But as the temperature rises, this gain effect gradually weakens and eventually disappears.

In addition to traditional micro–nano materials, DNA can also be used in the fabrication of thermal transistors due to its high bending flexibility [109] and isotropic thermal conductivity properties. Behnia and Panahinia [110]

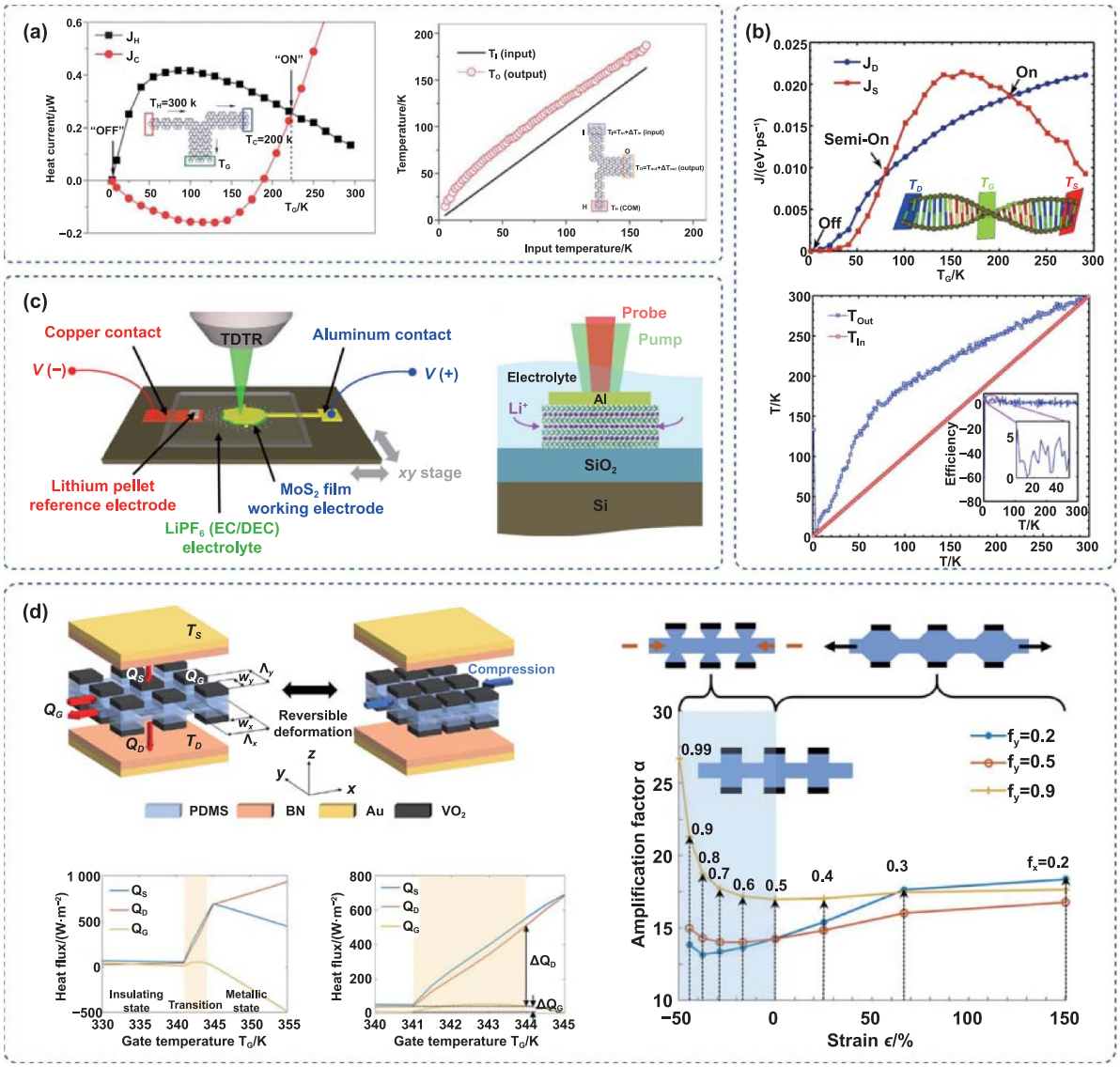

Figure 7. Simulation and experimental implementation of thermal transistors. (a) Three-terminal GNR. Reproduced from [108] with permission from the Royal Society of Chemistry. (b) DNA thermal transistor. Reprinted from [110], Copyright (2018), with permission from Elsevier. (c) Electrochemical thermal transistor. Reproduced from [15], with permission from Springer Nature. (d) Reconfigurable non-contact thermal transistor made of a phase-transition material. Reprinted from [111], Copyright (2021), with permission from Elsevier.

developed a high efficient DNA-based thermal transistor. The source, drain and gate of the transistor are connected by DNA molecular fragments with asymmetric sequence combination. As it is clear from figure 7(b), the on/off ratio of heat flow was as high as 700. The amplification factor reached about 64 at temperatures below 3 K and could reach about 6 at higher temperatures. In the ballistic regime, the reduction of the generalized correlation sum led to the increase of the phonon MFPs, which caused the increase of the thermal conductivity. It implies that the heat flux increased despite of decreasing temperature gradient. This is the NDTR.

Aside from directly controlling the thermal transistor through the gate temperature, the heat flux can also be modulated by methods such as dopant atoms and mechanical deformation. A thermal transistor based on MoS_2 thin films realized the switching of thermal transistors by electrochemical lithium intercalation and detachment [15]. Li intercalation would increase phonon–phonon scattering and thus reduce phonon lifetimes. Additionally, generating tensile strain along the *c*-axis would reduce phonon group velocities. Moreover, there was likely to be mixed 2H and 1T phases in MoS_2, and the disordered packing of the two would lead to the destruction of lattice periodicity, which also means increased phonon scattering. The superposition of the three effects made the intercalation of Li significantly inhibited the directional transmission of phonons, resulting in a sharp drop in thermal conductivity and realizing the switching of thermal transistors. The on/off ratio of lithium intercalation and deintercalation states was found to be about 8–10.

The phase-transition materials are also excellent candidates for the fabrication of thermal transistors due to the apparent

difference in properties between two phases. Chen *et al* [111] presented a dynamic-tuning non-contact thermal transistor with grating nanostructures. The gate terminal is comprised of vanadium dioxide (VO_2), a phase-transition material, and polydimethylsiloxane (PDMS), a soft material. In the phase transition region of VO_2, it was observed that the heat flow between source and drain could be markedly enhanced due to a small fluctuation of the gate heat flow (figure 7(d)). Moreover, the filling ratio can be changed by compressing or stretching the gate terminal, causing different radiative heat fluxes, thereby dynamically adjusting the amplification factor (figure 7(d)). The amplification factor varied from 12.8 to 26.7. In the phase-transition temperature range, the surface phonon polaritons (SPhPs) of the insulating VO_2 and the surface plasmon polaritons (SPPs) of the metallic VO_2 exhibit a strong local-field amplification effect on the radiative heat flow near the interfaces. The deformation of the grating will lead to the change of the SPhPs/SPPs modes and the coupling effects of the surface waves, thus resulting in the amplification effect of the thermal transistor.

Thermal transistors are very analogous to field effect transistors. The core of the devices is to construct NDTR effect, that is, to reduce the apparent average thermal conductivity at a higher temperature difference to obtain lower heat flow, so as to achieve the amplification effect. The physical mechanisms to achieve NDTR are summarized as follows: (1) intrinsic thermal conductivities decrease as temperature decreases. When thermal transistors adopt the strategy of fixing the hot bath temperature and lowering the cold bath temperature to increase the temperature difference, the average temperature of the thermal transistor itself is decreasing. If the resulting reduction in average thermal conductivity inhibits heat flow more than the gain in heat flow from an increase in temperature difference, the NDTR effect occurs. (2) Low-frequency transverse acoustic waves excited by phonon mismatch and large temperature difference at interfaces. When using a heterogeneous structure to construct a thermal transistor, the low-frequency transverse acoustic waves in the phonon spectrum are excited under large temperature differences and are easily reflected at the interface, which reduces the material's thermal conductivity. Meanwhile, as the gate temperature decreases, the matching degree of phonon power spectra declines, which not only offsets the gain effect of the temperature difference, but also leads to a decrease in heat flow. (3) Reduced phonon MFPs. Behnia and Panahinia [110] showed that when phonons are in ballistic regimes, the rise of generalized correlation sum under large temperature differences will lead to a decrease in MFPs of phonons, and the thermal conductivity will decrease. So reducing MFPs of phonons is a feasible way to construct NDTR. (4) Additional phonon scattering and decreased phonon group velocities. The research of Sood *et al* [15] showed that the intercalation of lithium in MoS_2 would increase phonon–phonon scattering and reduce the lifetimes of phonons, which signify that heat is more difficult to be transferred by phonons. Meanwhile, the tensile strain induced by Li intercalation would reduce the phonon group velocities to suppress the phonon transport. Both of these effects will lead to a decrease in thermal conductivity and thus NDTR. (5) Local-field enhancement effect. The study of Chen *et al* [111] showed that in the metal–insulator phase transition of VO_2, the local-field enhancement effect of SPhPs of insulating VO_2 and SPPs of metallic VO_2 amplified heat flow in thermal transistors.

Although researchers have theoretically built numerous models of thermal transistors and verified their functions, no rigorous experimental attempts of phonon-modulated thermal transistors have been found in the scope of this paper. Moreover, in the existing experimental studies, the function of thermal transistors can only be partially realized in limited and small temperature ranges, thereby dampening their potential for practical applications. Further analytical and experimental efforts are required to fully explore their capabilities. Thermal transistors that manipulate heat transfer using electrons such as [112, 113] have been put into practice. It is believed that once thermal transistors can be fabricated successfully, they will become one of the fundamental building blocks of thermal circuits and may be used to manage the operation of various phononic devices in the future.

3.3. Thermal memory

After the theoretical models of the thermal transistor were proposed, the thermal logic operation [75] and thermal memory [76] based on phonons have also been theoretically proved, which broadened the way for the development of phononics and laid the foundation for phonon-based information processing and computing. In order to record the two basic binary information of 0 and 1, thermal memory must contain nonlinear thermal devices to achieve at least two stable states.

Wang and Li [76] designed a nonlinear thermal device with a heat source, as shown in figure 8(a), which is a one-dimensional nonlinear lattice consisting of two Frenkel–Kontorova segments. When the temperature of the particle O was equal to T_{on} or T_{off}, the heat flow of the hot thermostat and the cold thermostat were equal and could maintain a steady state (as shown in figure 8(b)). In addition, the authors described the four working processes of this device in the article, including initialization, data writing, data storage and data reading. It was found that the device was stable when reading data, which means it can recover from the thermometer's not-very-small disturbance. The lifetime of data in thermal memory made of carbon nanomaterials was only about 100 μs. Although the lifetime is short compared to electronic dynamic random-access memory, the storage period can be considerably extended by amalgamating multiple identical thermal memories.

Phase-change materials are suitable to fabricate practical solid-state thermal memory devices. The principle is to utilize the metal–insulator transition in the phase transition temperature range to enhance the thermal conductivities of the devices, and then obtain the nonlinear and hysteresis response of temperature to achieve biostability. Xie *et al* [16] fabricated a thermal memory using a single-crystal VO_2 nanobeam. The results showed that the output temperature difference could be amplified by two orders of magnitude, while having good reproducibility and sensitivity. From the analysis

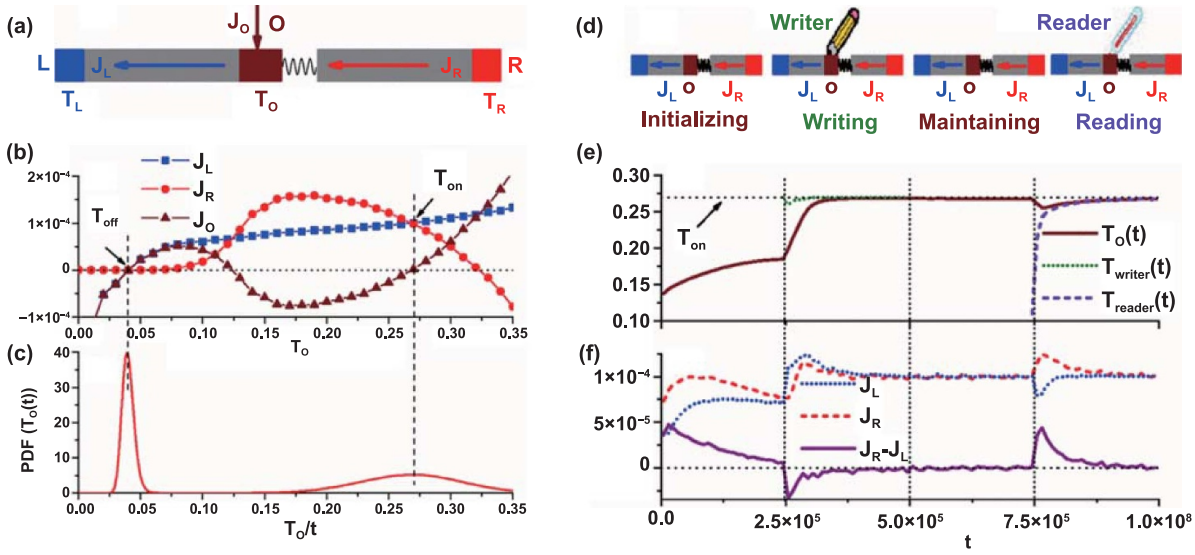

Figure 8. A theoretical model of thermal memories. (a) Configuration of the thermal memory. (b) Heat currents J_L, J_R and J_O versus the control temperature T_O. (c) Probability density function of the finite time temperature of the particle O in the absence of control heat bath. (d) Illustration of the four stages of a writing-reading process for an on state. (e) Temperatures of the particle T_O, writer T_{writer}, and reader T_{reader} as a function of time. (f) Heat currents J_L, J_R, and $J_R - J_L$ as a function of times. Reprinted figure with permission from [76], Copyright (2008) by the American Physical Society.

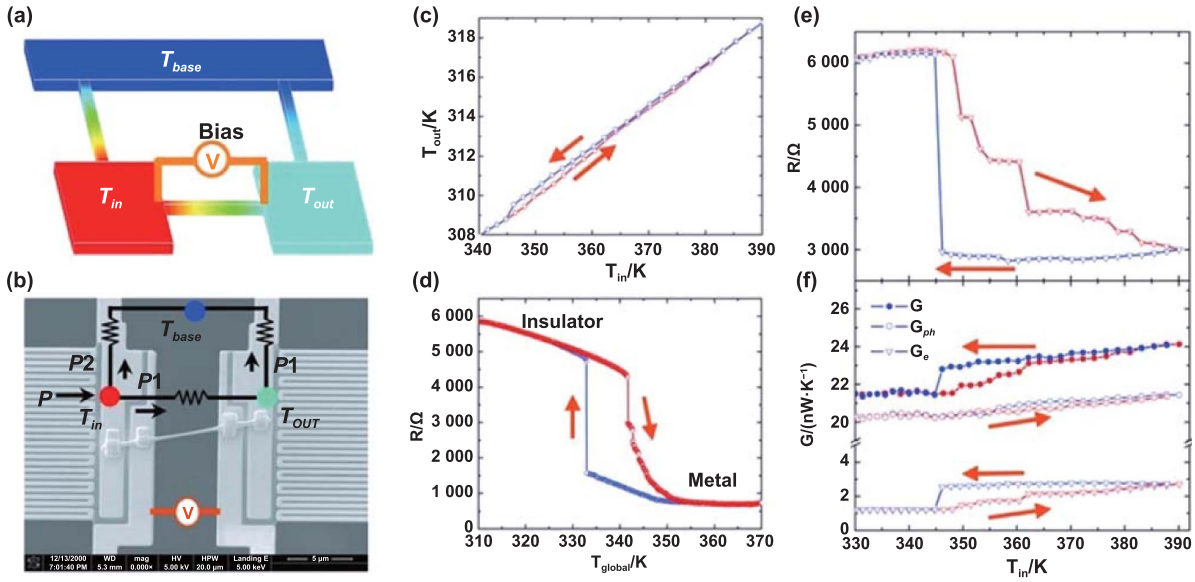

Figure 9. Schematic illustration (a) and SEM image (b) of the thermal memory device with an individual VO_2 nanobeam connecting the input terminal and output terminal. (c) T_{out} as a function of T_{in} without the application of a voltage bias upon heating (red curve) and cooling (blue curve). (d) Electrical resistance R of the nanobeam as a function of the global temperature with a uniform temperature distribution ($T_{global} = T_{in} = T_{out} = T_{base}$). (e) Electrical resistance R of the nanobeam under a temperature gradient as a function of T_{in}. (f) Total thermal conductance G, phonon contribution G_{ph} and electronic contribution G_e of the nanobeam as a function of T_{in} without the application of the voltage bias. [16] John Wiley & Sons. Copyright © 2011 WILEY-VCH Verlag GmbH & Co. KGaA, Weinheim.

of the contribution of electrons to thermal conductivity by the Wiedemann–Franz law, it can be known that although phonons dominate the heat conduction process, the hysteresis response of thermal conductivity mainly depends on electrons (figure 9(f)).

Thermal memories are capable of storing and reading temperature information. However, they may be undermined by thermal radiation and fluctuations, so more efforts are required to ensure the stability and reliability of the devices. Although the thermal bistability and hysteresis response in current studies are not predominantly determined by phonons, they still provide inspiration for future explorations. Manipulating thermal conductivity through phonon tuning is expected to become an effective method to obtain bistable temperature states and advance new solid-state thermal memories.

3.4. Thermoelectric device

Thermoelectric technology can realize the direct conversion of heat energy and electric energy, has no moving parts, and is clean and pollution-free, safe and reliable, so it has been widely used in space exploration [114], solar power generation [115], waste heat recovery [116], chip manufacturing [117], wearable devices [118] and many other fields, and is expected to become solutions to the challenges of energy woes [119]. The thermoelectric performance is evaluated by the thermoelectric figure of merit ZT, which is expressed as [120]

$$\mathrm{ZT} = \frac{TS^2\sigma}{\kappa} \tag{4}$$

where T is the temperature, S is the Seebeck coefficient, σ is the electrical conductivity, and κ is the thermal conductivity. Higher ZT values indicate superior thermoelectric conversion efficiency and better performance of thermoelectric devices, so finding or preparing thermoelectric materials with high ZT values has always been a crucial research focus in the field of thermoelectricity. For metals, since electrons play a major role in both electrical and thermal transport, the electrical and thermal conductivities of most metals obey the Wiedemann–Franz law

$$L = \frac{\kappa}{T\sigma} = \frac{\pi^2}{3}\left(\frac{k_\mathrm{B}}{e}\right)^2 = \mathrm{const} \tag{5}$$

where e is the elementary charge. Consequently, the ZT value of a metal is completely determined by the Seebeck coefficient. Since the Seebeck coefficients of metals are generally low, the conventional strategies prioritizing the optimization of the carrier concentrations have minimal effect on improving the ZT values. The above phenomena impede the search for materials with high ZT values in metals. For insulators, the low electrical conductivity hinders the efficiency of thermoelectric conversion, making it difficult to be applied in the field of thermoelectricity. The electrical conductivity of semiconductor materials is between that of metals and insulators, and owing to the fact that phonons and electrons jointly affect thermal conductivity, a higher ZT value can be obtained by regulating phonon transport to reduce thermal conductivity while retaining a high level of electrical conductivity. Structural modification at the nanoscale is the most effective way to enhance performance of thermoelectric conversion [121, 122]. Besides, with the development of miniaturization and integration of electronic devices, the application value of micro–nano scale thermoelectric devices is gradually increasing. Scholars have conducted extensive researches on how to improve the ZT values of micro–nano devices by manipulating the transport of phonons and electrons at the nanoscale. In the following, we will review some representative research progresses from the aspects of bulk nanostructured materials and low-dimensional nanomaterials.

3.4.1. Phonon engineering for bulk nanostructured materials. According to the kinetic theory, lattice thermal conductivity κ_L is expressed as

$$\kappa_\mathrm{L} = \frac{1}{3}c_\mathrm{v}v_\mathrm{g}^2\tau \tag{6}$$

where c_v is the specific heat, v_g is the phonon group velocity, and τ is the phonon relaxation time. Three effective strategies for minimizing thermal conductivity are obtained: (1) reducing the relaxation time by enhancing phonon scattering; (2) reducing the phonon group velocities; (3) reducing the specific heat.

Scattering sources exhibit frequency selectivity to phonons, and the frequency dependence varies between different sources, so appropriately selecting scattering sources according to specific scenarios can better accomplish desired outcomes. Point defects mainly include interstitials, vacancies and impurity atoms. They scatter as the fourth power of frequency, $\tau_\mathrm{PD} \sim \omega^{-4}$, which largely scatter high-frequency phonons [123]. Pei *et al* [124] embedded Ag_2Te uniformly into PbTe with some Ag cations distributed among a variety of interstitial sites that are tetrahedrally coordinated with Te atoms, so that the material showed a reduced lattice thermal conductivity. When the concentration of the dispersed phase increased, the thermal conductivity decreased further, signifying that more phonons were scattered due to the increased density of scattering centers. They [125] also carried out similar experiments in SnTe, introducing Cu atoms to replace Sn atoms and occupy interstitial sites. The enhanced phonon scattering reduced the thermal conductivity to $0.5\,\mathrm{Wm^{-1}\cdot K^{-1}}$, and therefore a peak ZT value, higher than 1, was achieved at 850 K. Compared with interstitial defects, vacancies are more dominant inherent point defects due to their low formation energy [126]. Li *et al* [127] found that Cu_2SnSe_4 with intrinsic vacancies at cationic sites had a thermal conductivity as low as $0.6\,\mathrm{Wm^{-1}\cdot K^{-1}}$, and a peak ZT around 0.6 could be achieved without additional technical approaches. Zhang *et al* [128] used Sb_2Te_3 as a solvent to form solid solutions with GeTe, so the hole concentration in GeTe was reduced to around the concentration required for optimal thermoelectric performances, and the resulting high concentration of vacancies and substitutions gave rise to strong phonon scattering, manifested by extremely low thermal conductivity. The final ZT was about 400% higher than that of pristine GeTe. Essentially, the phonon scattering caused by interstitial and vacancy defects is mostly induced by the strong mass and strain fluctuations around the vacancies or between host and guest atoms [129]. Such fluctuations broaden the dispersion curves and accelerate the phonon relaxation to return to the equilibrium state, which enhances phonon scattering and shortens phonon lifetime [130].

Linear defects or dislocations are another kind of efficient sources of phonon scattering, causing relaxation time, $\tau_\mathrm{D} \sim \omega^{-1}$, so as to scatter mid-frequency phonons [123]. Compared with 0D point defects, high-dimensional defects such as linear defects are conducive to enhancing phonon scattering without sacrificing carrier mobility [131]. Xin *et al* [132] found that high content of aliovalent Sb in Mg_2Si can introduce vacancies and dense dislocations. The combination of vacancies and dislocations led to a significantly lowered thermal conductivity. Meng *et al* [133] prepared Yb-filled

$CoSb_3$ materials with excess Sb content. The dense dislocation arrays inside the material reduced the thermal conductivity by 50%. This suppression combined with the increased Seebeck coefficient via energy filtering effect, dramatically increased the highest ZT to around 1.08. The aggregation of point defects can also generate dense dislocations in the grains of single-phase materials. Xu *et al* [134] reported that PbSe-based thermoelectric materials ($Pb_{1.02}Se_{0.72}Te_{0.20}S_{0.08}$–0.3%Cu) had a ZT value as high as 0.90 at low temperatures (300–573 K). Such remarkable thermoelectric performance originated from its exceptionally low lattice thermal conductivity. This work initially incorporated a large amount of Te and S alloying into PbSe to induce notable lattice distortion, and generate a strong strain field, which provides additional energy for dislocation formation. Then Cu interstitials were introduced to expedite formation of dislocations. Screw dislocations possess more obvious enhancement on phonon scattering than edge dislocations due to their larger strain field.

Interfacial defects are also concerned because of their strong scattering effect on low-frequency phonons ($\tau_{\mathrm{Inter}} \sim \omega^0$ [123]). Grain sizes reduction is a useful strategy for boosting interface density. Fu *et al* [135] introduced submicroscale grain boundaries into $Fe_{1.05}Nb_{0.75}Ti_{0.25}Sb$ compound, and plenty of atomic-scale point defects into the matrix to create hierarchical phonon scattering centers, which resulted in an 80% reduction in thermal conductivity and an improved ZT value of 1.34 at 1150 K. Mosaic crystals appear as single crystals macroscopically, but they are actually composed of numerous nanoscale crystallites of varying sizes and orientations, containing multiple small-angle grain boundaries [136, 137]. So, their thermoelectric properties are strengthened. He *et al* [138] applied the idea of nanoscale mosaicity in single-phase polycrystalline materials to realize simultaneous enhancement of multiple thermoelectric parameters. Besides the grain boundaries stated above, interface defects also include twin boundaries. Coherent twin boundaries can act as a deterrent to the selective scattering of mid-frequency phonons and low-energy carriers, which would increase the Seebeck coefficient while decreasing thermal conductivity. Lu *et al* [139] constructed dense twins and twin boundaries in Sn-doped Cu_3SbS_4 systems to enhance ZT values.

The lattice thermal conductivity also heavily depends on the phonon group velocity (V_g). In general, the overall group velocity is approximated as the velocity of sound (V_s), and it has been discovered that low sound velocity can result in low lattice thermal conductivity [17]. The phonon interaction is related to the characteristics and strength of chemical bonds. The sound velocity depends on these quantities by $V_s \sim \sqrt{k/M}$, where k represents the bonding strength, and M is the average mass. Weak chemical bonding and heavy constituent elements generally mean low sound velocities and lattice thermal conductivities. Ying *et al* [140] revealed that the poor lattice thermal conductivity in the non-cage structure α-MgAgSb originated from the combined effects of global and local weak chemical bonds. The global weak chemical bonds led to low sound velocity. The local vibrational modes induced by Mg–Ag–Sb three-centered bonds brought about low-frequency optical phonons, resulting in thermal damping that further reduced the lattice thermal conductivity. Hanus *et al* [141] also successfully applied the weak chemical bonding strategy in Na-doped PbTe materials. Since the stiffness of chemical bonds is inversely correlated with their length, an increase in lattice plane spacing generally corresponds to a decrease in bond strength and thus a change in phonon velocity. They increased the lattice plane spacing by internal inhomogeneous strain fields caused by lattice defects. Experimental results showed that the observed 7% reduction in the sound velocity in stoichiometric PbTe resulted in a 20% reduction in the thermal conductivity without introducing additional scattering sources. In contrast to phonon defect scattering which is approximately independent of temperature, the lattice softening mechanism works at all temperatures due to its temperature dependence.

Essentially, low specific heat can also achieve low thermal conductivity. Nevertheless, according to the Debye approximate model, the energy carried by each atom in a solid material is about $3k_BT$ at high temperature, so the high-temperature specific heat is close to the Dulong–Petit limit. It is quite challenging to minimize thermal conductivity through low specific heat. The emergence of superionic conductors provides a route to solve the problem. In the superionic phase, cations exhibit liquid-like diffusivity. In liquids, local atomic hopping and rearrangement suppress the propagation of shear waves and disrupt the thermal propagation of phonons, reducing the specific heat from $3Nk_B$ in typical solids to $2-2.5Nk_B$, where N is the number of particles. Liu *et al* [142] reported that the superionic conductor $Cu_{2-x}Se$ could achieve a high ZT value of 1.5 at 1000 K. The Se atoms in $Cu_{2-x}Se$ formed a rigid face-centered cubic lattice, and the copper ions were highly disordered around the Se sublattice with liquid-like mobility. Therefore, the partial liquid-like behavior in $Cu_{2-x}Se$ led to a dramatic reduction in the contribution of transverse phonon modes to the total specific heat, causing the specific heat to drop. ZT-enhanced performances have also been demonstrated in superionic conductors such as Cu_2S [143], $Cu_{2-y}Se_{0.5}S_{0.5}$ [144], and Ag_2Te [145].

For bulk nanostructured materials, the essential method to reduce thermal conductivity is to alter the lattice structures. For example, introducing defects can increase phonon scattering sources, and then reduce phonon relaxation time. Among the three defect forms, linear defects and planar defects are able to enhance phonon scattering without sacrificing carrier mobility compared with point defects. Meanwhile, due to the capability to selectively scatter low-energy carriers and mid-frequency phonons, planar defects are expected to increase the Seebeck coefficient while reducing thermal conductivity, which is a method with great potential. Apart from introducing defects, a lattice softening strategy to weaken the chemical bonding and reduce the phonon group velocity will also be an effective way to reduce the thermal conductivity. Superionic conductors realize the tuning of thermal conductivity from the perspective of specific heat. Generally speaking, these strategies can work synergistically on the material.

The coexistence of multiple scattering sources is beneficial to achieve scattering enhancement throughout the broad phonon spectrum to minimize relaxation time.

3.4.2. Phonon engineering of low-dimensional structures. While the above strategies have demonstrated effectiveness in 3D materials, there are still challenges to overcome, particularly the inverse relationship between the Seebeck coefficient and electrical conductivity with changes in carrier concentration, which ultimately restricts the increase of ZT values [146]. In the late 1990s, Hicks and Dresselhaus [147] proposed the concept of improving thermoelectric performance through low-dimensionality. Low-dimensionality helps increase the electronic DOS near the Fermi level, causing an increase in the Seebeck coefficient. And it can also strengthen the phonon scattering without significantly increasing the electron scattering at surfaces, thereby reducing the thermal conductivity of the material without affecting the electrical conductivity [148]. So, it points out a new path for finding materials with high ZT values. From the above, two strategies to enhance the thermoelectric properties of materials at the nanoscale are acquired: (1) enhancing DOS near the Fermi level by quantum confinement effects to enhance power factor [149–152]; (2) reducing thermal conductivity by phonon tuning approaches [18, 19, 153–159]. The latter strategy is mainly discussed within the scope of this paper. Researchers have designed various new thermoelectric materials with microstructure characteristics such as superlattices [105, 154–156], nanocomposites [18, 157], nano porous materials [19, 158], nanowires [159] etc, which are favorable to significantly reduce the thermal conductivity of materials and exhibit excellent thermoelectric performance.

3.4.2.1. Superlattices. A superlattice thin film is a periodic structure formed by stacking layers of two or more materials, in which the thickness of each layer usually ranges from a few to tens of atomic layers. In superlattices, phonon transport may exhibit particle-like or wave-like properties [160]. If the MFP of phonons is shorter than the thickness of one period, phonons exhibit particle-like behaviors, and the phonon propagation within each layer and interfacial scattering do not interfere with each other. Experimental results can be well explained using particle-based physical models. In this case, thermal conductivity can be reduced by augmenting phonon scattering through increasing the interface roughness and density, introducing impurity particles, and increasing the mismatch degree of phonon DOS between different layers. Ge/Si/Ge/Si/Ge composite quantum dots (figure 10(b)) prepared by Chang *et al* [154] exhibited a highly reduced thermal conductivity of $5-7.5\ \mathrm{Wm^{-1}\cdot K^{-1}}$, a factor of 25 lower than that of bulk Si, which was attributed to the enhanced phonon scattering caused by the high Si/Ge interface density and increased local SiGe alloying. Vaziri *et al* [155] realized the artificial stacks of single-layer graphene, MoS_2 and WSe_2, obtaining $Gr/MoS_2/WSe_2$ heterostructure with a thickness less than 2 nm. But the total thermal resistance of the heterostructure was comparable to that of silicon dioxide with a thickness of 300 nm. At room temperature, the effective thermal conductivity was only $0.007-0.009\ \mathrm{Wm^{-1}\cdot K^{-1}}$, about one third of the thermal conductivity of air. When the phonon MFP is equal to or longer than the periodic thickness, the wave characteristics of phonons need to be considered. Under this circumstance, phonons can be coherently transmitted over a distance of several periods without losing phase information and reflected at multiple interfaces, causing interference effects [160]. Phonon coherence will modify phonon dispersion relations, thus forming or expanding phononic bandgap, and reducing the phonon group velocities [161]. Furthermore, if aperiodicity is introduced into superlattices, the heat transport ability of coherent phonons can be weakened, and may induce phonon localization, enabling the structures to achieve ultrahigh thermal isolation [105, 162, 163]. Note that to observe this effect of phonon coherence, the superlattice interfaces should be of high quality [164]. Luckyanova *et al* [105] destroyed the periodic structures by adding ErAs nanodots with sizes comparable to the wavelengths of coherent phonons that dominates heat transport in GaAs/AlAs superlattices, leading to the localized behavior of phonons and decreased thermal conductivities. Venkatasubramanian *et al* [156] reported that the ZT value of p-type Bi_2Te_3/Sb_2Te_3 ultra-short-period superlattice thin film devices could reach a maximum of about 2.4. Such enhancement was achieved by controlling the transport of phonons and electrons in the superlattices. The ultra-short-period superlattices maintained high levels of in-plane carrier mobilities and cross-plane conductance due to the near absence of alloy scattering and random interfacial carrier scattering. For thermal conductivity, the diffusion transport analysis showed that there was a low-frequency cutoff in the phonon spectrum, which suggested that low-frequency phonons were suppressed for transport, indicating localization-like behaviors.

3.4.2.2. Nanocomposites. Nanocomposites generally refer to nano-heterostructures obtained by incorporating nano-inclusions into a matrix [165, 166]. Nano-inclusions, such as fine grains and nanoparticles, provide an additional scattering mechanism for phonons. At the same time, if nano-inclusions are semi-metals or metals, they could be used as electron donors to improve the electrical conductivity of the material. Consequently, the thermoelectric properties of alloy matrixes embedded with nano-inclusions are enhanced. Kim *et al* [157] found that compared with pure $In_{0.53}Ga_{0.47}As$, the $In_{0.53}Ga_{0.47}As$ film embedded with ErAs nanoparticles showed a thermal conductivity reduction effect in a wide temperature range, and the reduction was the largest between 150 K and 450 K, almost a factor of 2 below the alloy limit, resulting in a more than two-fold increase in ZT. It is worth noting that for the take of reducing thermal conductivity, the size of ErAs nanoparticles should be large enough that the enhanced scattering regime does not overlap with the Rayleigh scattering region enhanced by atomic-scale defects in the alloys. In alloys, owing to the difference in mass and/or bond stiffness between the constituent elements, atomic substitution primarily scatters short-wavelength phonons or Brillouin zone edge phonons, so mid- and long-wavelength phonons play a

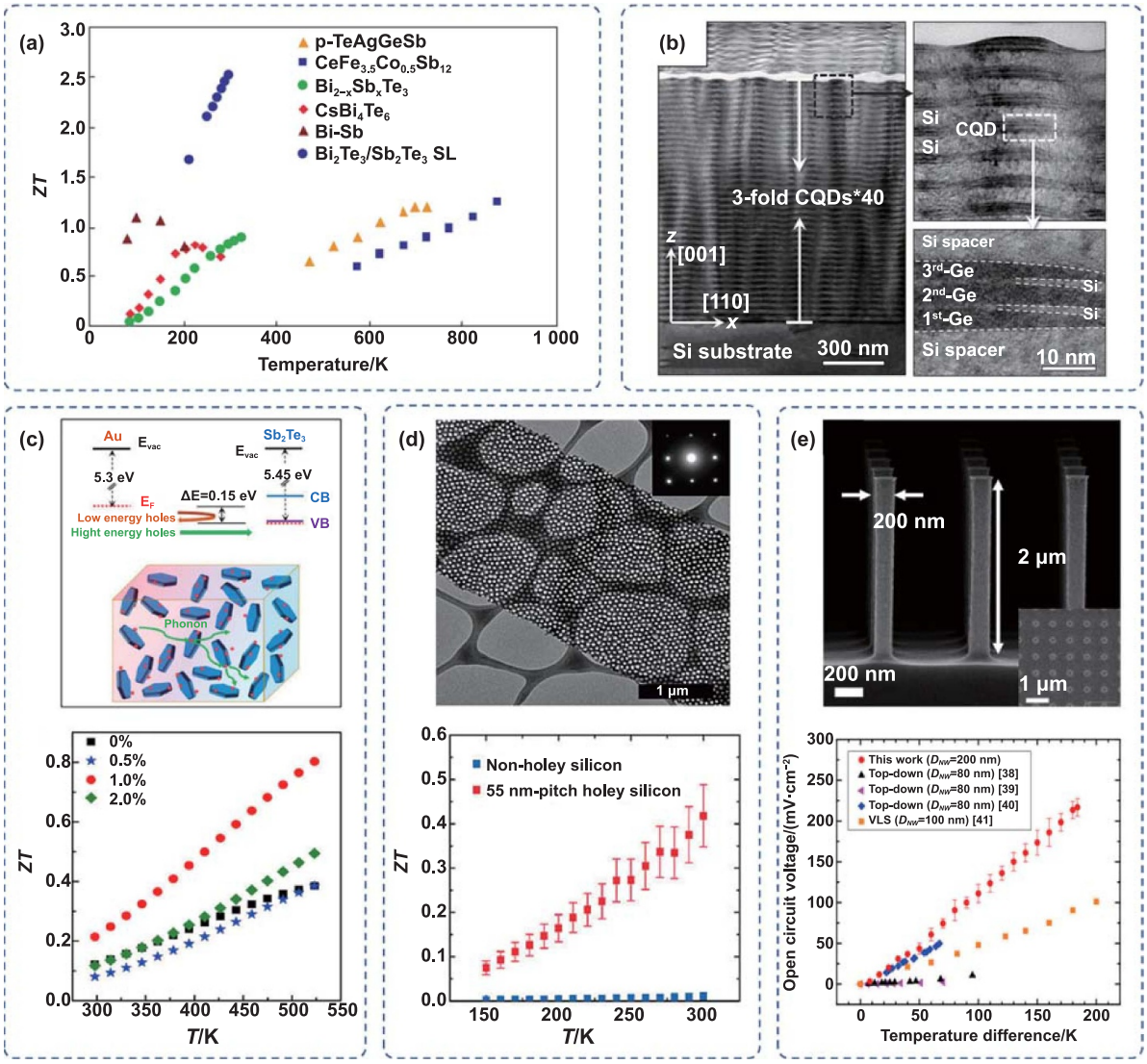

Figure 10. Enhancement of thermoelectric performances based on low-dimensional structures. (a) Temperature dependence of ZT of p-type Bi_2Te_3/Sb_2Te_3 superlattice compared to those of several recently reported materials. Reproduced from [156], with permission from Springer Nature. (b) Thin-film-like Ge/Si/Ge composite quantum dots. Reprinted from [154], with the permission of AIP Publishing. (c) 0D–2D Au–Sb_2Te_3 nanocomposites. Reprinted with permission from [18]. Copyright (2019) American Chemical Society. (d) Holey silicon ribbons. Reprinted with permission from [19]. Copyright (2010) American Chemical Society. (e) Vertical Si-NWs arrays. Reprinted with permission from [159]. Copyright (2019) American Chemical Society.

dominant role in heat conduction. Similarly, Zheng *et al* [18] constructed a hybrid 0D–2D nano-heterostructure by growing Au nanoparticles *in situ* on the hexagonal Sb_2Te_3 nanoplates, which realized simultaneous optimization of three thermoelectric parameters including electrical conductivity, thermal conductivity and Seebeck coefficient. Thus, the ZT value was improved by 110% compared with that of pristine Sb_2Te_3.

3.4.2.3. Nano porous materials. Nano porous materials have been proved to be high-performance thermoelectric materials, which regulate thermal conductivity via designing pore shapes, pore sizes, and porosities [167, 168]. Phonon specular backscattering at the sidewalls of high-density holes is mainly responsible for thermal conductivity reduction. Especially when the distance between adjacent holes is smaller than the phonon MFP, the phonons will be 'trapped' behind the holes, resulting in a local negative temperature gradient opposite to the linear temperature gradient along a free channel. Tang *et al* [19] investigated the thermoelectric properties of single-crystal silicon films decorated with high-density nanoscopic holes. At room temperature, the holey silicon ribbons showed a suppression of thermal conductivity by a factor of 34 compared to nonporous silicon ribbons. The experimental results showed that the thermal conductivity decreased with the increase of the neck width, that is, a thinner neck will induce a stronger necking effect and lower overall thermal conductivity. In the entire range of experimental temperatures, the ZT value was enhanced by about 50 times, 0.4 at 300 K, compared with that of nonporous silicon of the same

Table 2. Summary of the performance of phonon-engineered thermoelectric nanomaterials in different studies.

Physical mechanism	Materials	ZT	Authors	Time
Enhanced scattering	$Na_{0.03}Eu_{0.03}Cd_{0.03}Pb_{0.91}Te$	2.5	Wu *et al* [130]	2020
	$Bi_{0.07}Ge_{0.90}Te$	2.3	Jiang *et al* [131]	2022
	$Ge_{0.76}Sb_{0.08}Pb_{0.12}Te$	2.3	Zhang *et al* [128]	2018
	$Cu_2S_{0.52}Te_{0.48}$	2.1	He *et al* [138]	2015
	Cu_2Se	1.9	Zhao *et al* [167]	2017
	La-doped *n*-type PbTe–Ag_2Te	1.6	Pei *et al* [124]	2011
	$Fe_{1.05}Nb_{0.75}Ti_{0.25}Sb$	1.34	Fu *et al* [135]	2016
	$Bi_{0.3}Sb_{1.7}Te_3$ + 0.4 vol% SiC	1.33	Li *et al* [166]	2013
	Yb-filled $CoSb_3$	1.08	Meng *et al* [133]	2017
	$Sn_{0.94}Cu_{0.12}Te$	1.0	Pei *et al* [125]	2016
	$Pb_{1.02}Se_{0.72}Te_{0.20}S_{0.08}$–0.3%Cu	0.96	Xu *et al* [134]	2022
	$Cu_3Sb_{0.985}Sn_{0.015}S_4$	0.76	Lu *et al* [139]	2022
	Nanoporous Bi_2Te_3	0.67	Qiao *et al* [168]	2019
	Cu_2SnSe_4	0.6	Li *et al* [127]	2016
	Rough Si nanowires	0.6	Hochbaum *et al* [169]	2008
Liquid-like behavior	$Cu_{1.94}Se_{0.5}S_{0.5}$	2.3	Zhao *et al* [144]	2017
	$Cu_{1.97}Se$	1.7	He *et al* [143]	2014
	β-phase Cu_2Se	1.5	Liu *et al* [142]	2012
	Ag_2Te	1.2	Jakhar *et al* [145]	2022
Phonon localization	Bi_2Te_3/Sb_2Te_3 superlattice	2.4	Venkatasubramanian *et al* [156]	2001
	Au–Sb_2Te_3	0.8	Zheng *et al* [18]	2019
	Holey silicon	0.4	Tang *et al* [19]	2010
	$Si_{0.8}Ge_{0.2}$	0.08	Perez-Taborda *et al* [158]	2016

thickness. Analogously, Perez-Taborda *et al* [158] fabricated $Si_{0.8}Ge_{0.2}$ porous nano meshed films by DC sputtering on highly ordered porous alumina substrates. Due to alloying, and phonon scattering on the upper/lower boundaries and crystallite boundaries within the nano-meshes, a slump in the thermal conductivity was observed. And the thermal conductivity decreased as the hole diameter became smaller, down to $(0.55 \pm 0.10)\,\mathrm{Wm^{-1} \cdot K^{-1}}$, well below the amorphous limit. For nano meshed films with pores of larger diameters, the ZT values could reach around 0.08 at room temperature.

3.4.2.4. Nanowires. Nanowires are typical one-dimensional materials that have much smaller feature sizes than bulk materials. As a result, phonon transport in nanowires is restricted by their boundaries. Silicon nanowires have garnered significant attention in the field of thermoelectricity due to the considerable variation in MFPs between electrons and phonons at room temperature [169]. Lee *et al* [159] significantly reduced the thermal conductivity of silicon nanowires by rational incorporation of phonon scattering sources at several scales. Diameter reduction makes phonon scattering stronger in all wavelength ranges, reducing the MFPs of full-wavelength phonons; surface roughness causes additional phonon scattering, reducing the MFPs of long-wavelength phonons; the presence of impurities atoms also causes additional scattering of phonons. The superposition of the three effects will obviously inhibit the thermal conductivity of Si-NWs. Boron-doped Si-NWs with a surface roughness of 6.88 nm and a diameter of 200 nm exhibited the lowest thermal conductivity, which was 5.1 times lower than that of smooth intrinsic nanowires and 14.8 times lower than that of bulk silicon. The performance of the thermoelectric modules based on the doped rough Si-NWs arrays was better than all known Si-NW thermoelectric modules.

To sum up, as a solution for micro–nano-scale and flexible thermoelectric devices, low-dimensional nanomaterials currently mainly adopt the strategy of enhancing phonon scattering to reduce thermal conductivity (table 2). Superlattices and nano porous materials primarily increase interface and boundary scattering, while nanocomposites and nanowires mainly increase impurity scattering. Due to quantum confinement in low-dimensional materials, numerous studies have combined electronic band engineering with multiscale phonon engineering, with the aim of simultaneously optimizing both electron and phonon transport for high thermoelectric performances [18, 156, 170]. Thermoelectric figures of merit have already reached an equivalent level to that of bulk thermoelectric materials. However, the preparation of low-dimensional thermoelectric materials requires high-precision processing and preparation technologies, which have strict requirements for experimental conditions and environments, and are complicated and costly, thus they are still far from practical applications.

In the performance enhancement of thermoelectric devices, the major objective of phonon tuning is to achieve remarkable decrease in thermal conductivities. In the above review, we enumerated various approaches to reduce thermal conductivity by modifying phonon transport. The main strategies and their physical mechanisms are summarized as follows: (1) enhanced scattering. Point defects, linear dislocations, and

interfacial defects in bulk materials, as well as interfaces, boundaries, disorders in low-dimensional materials are all additional phonon scattering sources, and the scattering probability of each type of scattering source has its own frequency dependence, which can suppress phonon transport in different frequency ranges. Moreover, a rational combination of different scattering sources can achieve enhanced phonon scattering in a wider frequency range, showing a further reduction in thermal conductivity, such as the vertical silicon nanowire study of Lee *et al* [159]. (2) Phonon localization. Inducing one-way phonon localization is one of the approaches to induce thermal rectification effect. Localized phonons can also be used to suppress heat transport in the thermoelectric field. The ultra-short-period superlattice structure prepared by Venkatasubramanian *et al* [156] exhibited localized behavior of low-frequency phonons due to coherent backscattering at the interfaces. The necking effect in the study of Tang *et al* [19] can actually be regarded as a phonon localization phenomenon, since phonons are unable to conduct heat effectively in this case. (3) Lattice softening. The bonding properties of chemical bonds in crystals have a profound impact on phonon interactions. As the medium changes from gas to liquid, then to solid, the chemical bonds between the constituent atoms become stronger and sound waves travel faster, roughly indicating lower phonon velocities in weakly bonded systems. Many experimental results also manifest that weak chemical bonds are an important factor leading to low sound velocities and low thermal conductivities. For example, Hanus *et al* [141] observed a 7% reduction in the sound velocity and a 20% reduction in the thermal conductivity in lattice-softened stoichiometric PbTe. (4) Liquid-like behavior. Liquids exhibit reduced specific heat due to the suppression of transverse phonon modes caused by local atomic hopping and rearrangements. If solid materials can possess liquid-like mobility, low thermal conductivity can be easily achieved through low specific heat. The cations in superionic crystals reported by Liu *et al* [142] were highly disordered and exhibited liquid-like fluidity, resulting in a substantial decrease in thermal conductivity.

3.5. Thermal cloak

The concept of thermal cloak was first proposed by Fan *et al* in 2008 [171], the main features are inverse thermal flow and thermal shielding effect. In 2012, Guenneau *et al* [172] further developed the concept of thermal cloak, that is, on the basis of thermal shielding, to achieve thermal stealth. Thermal stealth involves ensuring that the temperature distribution outside the cloak remains unchanged, so that objects inside the cloak cannot be detected through temperature detection. The common structure of thermal cloaks is the core–shell structure. To make the materials inside the core invisible, the thermal conductivity of the shell is required to be anisotropic and non-uniform to meet specific spatial variation laws, or the shape of the shell needs to be a special geometric structure. Guenneau *et al* applied the method of transformation optics to the field of thermodynamics, carried out coordinate transformation on the heat conduction equation, and constructed a cylinder with non-uniform and anisotropic thermal conductivity as a thermal cloak. The simulation results proved that the thermal cloak could ensure that the temperature inside the cloak was uniform and did not exceed half of the normalized temperature without changing the external temperature distribution.

However, experimentally preparing such anisotropic thermal metamaterials is a huge challenge. An effective solution is to form periodic alternating structures with various homogeneous, non-singular and isotropic materials. In 2013, Han *et al* [173] demonstrated the effectiveness of this strategy through theoretical analysis and full-wave simulations. In the same year, Schittny *et al* [20] experimentally designed a periodically alternating copper-PDMS composite structure, as shown in figure 11(b). The experimental results showed that the temperature of the area inside the thermal cloak was much lower than the surrounding area, which indicated that the thermal cloak had a good thermal insulation effect. In addition, a simple double-layer thermal cloak was also experimentally demonstrated by Han *et al* [174] to achieve thermal stealth. Based on this double-layer thermal cloak structure, Han *et al* [175] designed a thermal camouflage device that can hide the thermal properties of any object and disguise it as another object. However, this structure theoretically requires the thermal conductivity of the inner layer material to be zero, which cannot be achieved in experiments, so there is still a distance for its application. In recent years, 3D printing technology and topology optimization theory have provided new approaches for realizing thermal metamaterials with complex thermal conductivity distributions. Sha *et al* [176] adopted multi-scale topology optimization design and used 3D printing to fabricate anisotropic thermal metamaterials, and proposed a design strategy for thermal cloaks with freeform shape and omnidirectional functionality. The experimental results proved that the devices could realize both thermal stealth and thermal sensing functions, freeing the thermal cloak from the shackles of regular shape design.

At the macro scale, most of the designs of thermal cloaks have strict requirements on the distribution of thermal conductivity, or use periodic alternating composite structures, but these designs are difficult to implement at the micro–nano scale. The reason is that non-uniform anisotropic thermal conductivity is knotty to achieve at the nanoscale, and the periodic alternation of multilayer materials will introduce a large number of boundaries, making phonon boundary scattering and interfacial thermal resistance non-negligible. In 2016, Ye and Cao [177] reported the nanoscale thermal cloak design for the first time, which partially chemically modified graphene to achieve the thermal cloak effect. The structure is shown in figure 11(d). The yellow ring region is the thermal cloak, which is graphene chemically modified with hydrogen, methyl or hydroxyl, and the rest of the area is unmodified graphene. The introduction of chemical functional groups on graphene caused chemical bonds transforming from sp^2 to sp^3, and led to phonon localization, so that the heat flow avoided the thermal cloak area and achieved a partial thermal cloaking effect. Although the hydrogenated graphene cloak cannot achieve perfect thermal stealth, it had better thermal shielding and stealth effects than defect graphene and hollow

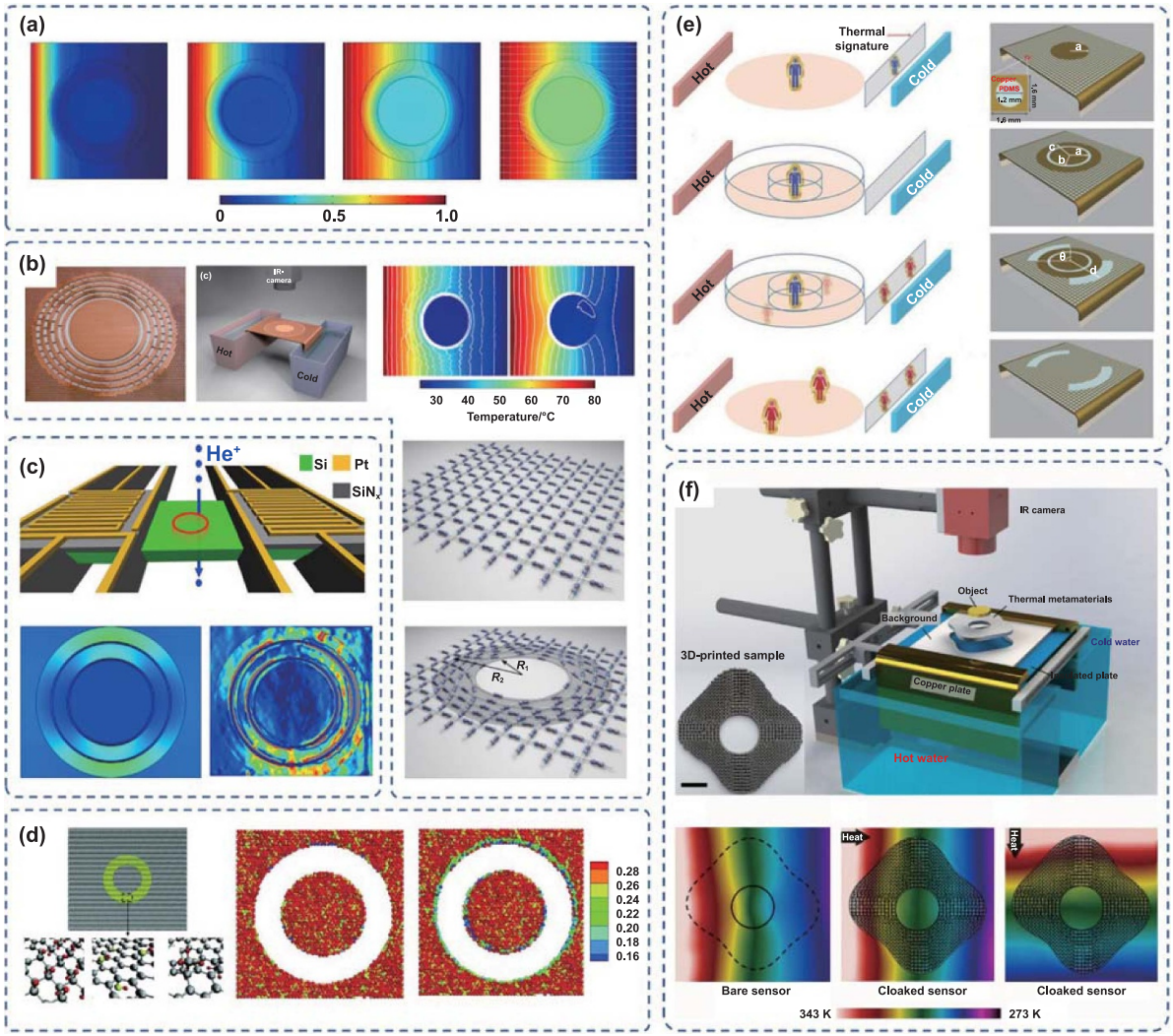

Figure 11. Simulation and experimental implementation of thermal cloaks. (a) Diffusion of heat from the left on a cloak. Reprinted with permission from [172] © The optical Society. (b) Microstructured thermal cloak. Reprinted figure with permission from [20], Copyright (2013) by the American Physical Society. (c) Writing of local thermal conductivity in suspended single-crystal Si membrane using the He^+ ion beam. Reprinted with permission from [178]. Copyright (2019) American Chemical Society. (d) Thermal cloaking in chemically modified graphene. Reproduced from [177] with permission from the Royal Society of Chemistry. (e) Thermal camouflage. [175] John Wiley & Sons. © 2014 WILEY-VCH Verlag GmbH & Co. KGaA, Weinheim. (f) Thermal cloaks with freeform shape and omnidirectional functionality. Reprinted from [176], Copyright (2022), with permission from Elsevier.

graphene. In addition, modification with higher molecular weight functional groups can significantly improve the thermal cloak performance. Compared with hydrogen atoms, methyl and hydroxyl modification can increase RTC (ratio of thermal cloaking, the ratio of heat flow inside and outside the cloak) by 16.5% and 60.5%, respectively.

At present, most of the design ideas of nanoscale thermal cloaks lie in regulating the thermal conductivity of designated regions. In addition to chemical modification methods, annealing proved to be a highly feasible strategy. In 2019, Liu *et al* [179] constructed thermal cloaks by annealing silicon films *in situ*. The basic principle is that annealing amorphizes the silicon in the ring area, thereby greatly reducing the thermal conductivity from the intrinsic value ($\sim$50 $Wm^{-1} \cdot K^{-1}$) to the amorphous value ($\sim$1.7 $Wm^{-1} \cdot K^{-1}$), and forming a thermal cloak. The MD simulation results showed that the RTC of the thermal cloak could reach 5.2, and the shielding performance was proportional to the width of the cloak ring. By calculating the phonon DOS and the mode participation rate, Liu *et al* found that most of the phonon modes in crystalline silicon films were delocalized. For the silicon membrane inside the cloak ring, the localization of phonons was obvious, which was the reason for the decrease of the thermal conductivity of amorphous silicon and the potential mechanism of thermal cloaking.

In the same year, Choe *et al* [178] designed the ion-write microthermotics (IWMT), which can partially, continuously and reversibly amorphize the suspended silicon film, and has a good spatial resolution (10–100 nm). Figure 11(c) shows a schematic diagram of the IWMT device. Choe *et al* prepared a four-layer thermal cloak by the device, and observed the thermal stealth effect at the microscopic scale for the first time.

The temperature distribution of the finite-element method simulations and experiments are shown in figure 11(c), respectively. Experimental measurements showed that the thermal cloak reduced the heat flow in the cloaking area to one-fifth of the original, indicating a good thermal stealth effect. Furthermore, MD simulation results showed that the thermal cloak designed by the IWMT platform was insensitive to interfacial thermal resistance, which made the IWMT platform more attractive.

Perfect thermal stealth is one of the most desired goals of thermal cloaks. At the macroscale, perfect thermal stealth requires thermal metamaterials with non-uniform and anisotropic thermal conductivities [172]. In practical applications, two or more homogeneous and isotropic materials with different thermal conductivities can be used instead, and experiments have proved that they have excellent thermal stealth effects [20, 173]. At the microscopic scale, methods such as chemical modification [177], annealing [178, 179], punching [180] can be utilized to adjust the thermal conductivity of a specific region to form a thermal cloak. A number of studies have shown that the core mechanism of the micro–nano scale thermal cloak is phonon localization [177–180], which is responsible for the decrease in the apparent thermal conductivity of the thermal cloak region. Phonon localization makes heat flux avoid the thermal cloak area to achieve the thermal stealth effect. The difficulty in designing thermal cloaks at the microscopic scale lies in precise thermal conductivity control and overcoming the negative effects of phonon boundary scattering and interfacial thermal resistance. In the future, more phonon manipulation methods, such as coherent scattering and augmenting the number of scattering centers, are expected to provide new ideas for the design of thermal cloaks.

4. Summary and future development direction

This paper reviews recent advances in phonon engineering, and highlights the practical applications of phonon manipulation in fields of thermal rectification, thermal transistors, thermal memories, thermoelectric devices and thermal cloaks at the nanoscale. As the essence and core of phonon engineering, the adjustment of phonon dispersion relationship can directly affect the phonon DOS and then change the overall physical properties. Through different phonon regulation methods, including matching/mismatching of phonon power spectra, phonon localization, increasing/decreasing phonon scattering, and changing phonon group velocities, etc, we can obtain special physical properties to achieve target functions. For example, thermal rectification phenomena can be observed by inducing one-way phonon localization, constructing asymmetric phonon scattering, and promoting mismatch of phonon power spectra. Another example is to construct NDTR, the key to thermal transistors, by reducing the phonon MFPs and group velocities, and exciting low-frequency horizontal transverse acoustic waves.

Electronics are the fundamental elements underpinning the development of modern science and technology. While showing great advantages, they also have the shortcoming of high-power consumption. Logical devices based on phonon transport can not only realize the direct extraction, storage and transmission of thermal signals, but also can be combined with traditional electronic circuits for better thermal management of devices, which is a promising development direction. So far, although scholars have carried out numerous researches in the field of phonon modulation and harvested many uplifting results, and have also proposed plenty of theories to describe and explain the observed phenomena such as acoustic mismatch theory [181, 182], Anderson localization of phonons [183, 184], ballistic thermal transport [185, 186], etc, there are still large gaps in our understanding of electron and phonon transport mechanisms. Further research into mechanisms of phonon transport is of fundamental importance and may make it accelerate to become reality for phonons to carry and process information.

Within the scope of this review, only thermal rectifiers and thermoelectric devices have more experimental studies, while thermal transistors, thermal memories and thermal cloaks are mostly theoretical, and experimental research is still in its infancy. On the one hand, the realization of the functions of phononic devices often requires special materials or complex structures, which put forward extremely high requirements for micro–nano processing technology. On the other hand, the concepts and models of the thermal transistors, thermal memories and thermal cloaks are still new, and it has not been more than 20 years since they were proposed, so their development is still immature. Therefore, the performances of most phononic devices have yet to be tested in reality. More experiments are needed to prove the feasibility of phononic devices in the future. The methods of phonon regulation at the nanoscale reviewed in this work are anticipated to provide extended ideas for the above researches. In addition, although the materials and structures that can realize thermal rectification are very abundant, there are very few that are actually transformed into practical application devices. More practical thermal rectification devices are the goals that scholars need to pay more attention to. Further examining the analogies between thermal and electrical components, richer functions can be achieved by constructing thermal circuits similar to commonly used electrical circuits, for instance, using multiple thermal rectifiers in parallel to construct thermal diodes with greater output heat flow, utilizing thermal logic gates to perform intricate logic operations, using thermal diodes to construct thermal peak detectors [187], and employing thermal transistors to realize thermal mixers [187], etc.

Traditional thermal performance adjustments are often achieved through complex structural designs. Nevertheless, it has always been a challenge to quickly obtain the optimal structure and chemical composition with target properties due to the fact that the design of nanostructures or atomic structures has the characteristics of large selectivity for parameters, high degree of freedom, and excessive time and economic costs associated with structure search and subsequent experimental verification. The emergence of materials informatics [188] can assist in material discovery and structure optimization gradually transforming from traditional and slow trial-and-error strategies to efficient high-throughput screening

from the pool of candidate materials [189], which have been applied in structural design in fields of thermal metamaterials [163, 190, 191], thermoelectric conversion [188, 192, 193], thermal manipulation [194, 195], etc. Hu *et al* [190] used machine learning to search for globally optimal aperiodic superlattice structures with minimized coherent phonon heat conduction. Yamawaki *et al* [188] performed structural optimization of GNRs by alternating multifunctional (phonon and electron) transport calculations and Bayesian optimization, improving the thermoelectric figure of merit of graphene by a factor of 11. Ji *et al* [194] established an artificial neural network to learn and predict the stealth effect of thermal cloaks. Therefore, the application of machine learning in thermal science has extraordinarily high research value and practical significance, which can accelerate the pace of material discovery and enable rapid and effective structure optimization.

Once the material is prepared, its thermal characteristics are fixed and can only be applied to a single scene. Whereas in some fields, the application scenarios and requirements of devices may be constantly changing. For instance, electronic chips need good heat dissipation when they work at high power, but in environments of low temperatures, in order to ensure normal functions, the chip temperature needs to be kept within an appropriate range. Therefore, the development of devices whose intrinsic properties can be adjusted on demand is a promising research direction. Sood *et al* [15] achieved controllable adjustment of the thermal conductivity of MoS_2 thin films by reversible electrochemical lithium intercalation and detachment. Lu *et al* [196] oxygenated or hydrogenated $SrCoO_{2.5}$ by electrochemical methods to achieve bidirectional control of thermal conductivity in the range of nearly 10 ± 4 folds at room temperature. Zhang *et al* [197] utilized an external magnetic field to affect phonon transport through spin–phonon interactions, breaking the symmetry of heat transport and realizing thermal rectification. In the future, exploring the regulating effect of external fields (including electric field, magnetic field, temperature field, etc) on phonon transport is expected to expand beyond original design methods and provide a new development direction for devices with adjustable performance.

Combining phonon modulation with electronic or photonic modulation probably leads to beneficial applications. Because of the complexity of thermoelectric materials, the optimization of a single parameter may have adverse effects on other parameters. Therefore, in the literatures reviewed in the thermoelectric part of this paper, in addition to reducing thermal conductivity by phonon engineering, some of them combined electronic energy band engineering to synergistically optimize thermoelectric figure of merit, hence a higher thermoelectric conversion efficiency is obtained. Phonons and photons can also be co-managed. Maldovan and Thomas [198] tuned acoustic and light waves simultaneously in two-dimensional periodic structures to localize photons and phonons at the same time. This localized state can strongly affect the photon–phonon interactions, offering possibilities for acoustic-optical devices that manage sound, light, and heat comprehensively. With the ongoing development of computational methods, it is possible now to calculate material properties taking into account interactions between electrons, photons and phonons. This will allow simultaneous optimization of electrical, optical and thermal properties of multifunctional materials, enabling the corresponding devices to have more excellent and comprehensive performance.

Acknowledgments

This work was supported by the National Natural Science Foundation of China Grant Nos. 52276072 and 51976096.

ORCID iDs

Siqi Xie https://orcid.org/0009-0002-2626-3004
Hongxin Zhu https://orcid.org/0009-0002-8178-729X

References

[1] Pokatilov E P, Nika D L and Balandin A A 2005 Acoustic phonon engineering in coated cylindrical nanowires *Superlattices Microstruct.* **38** 168–83
[2] Mori N and Ando T 1989 Electron-optical-phonon interaction in single and double heterostructures *Phys. Rev.* B **40** 6175–88
[3] Giustino F 2017 Electron-phonon interactions from first principles *Rev. Mod. Phys.* **89** 015003
[4] Regner K T, Sellan D P, Su Z H, Amon C H, Mcgaughey A J H and Malen J A 2013 Broadband phonon mean free path contributions to thermal conductivity measured using frequency domain thermoreflectance *Nat. Commun.* **4** 1640
[5] Chen M Y, Lin X, Dinh T H, Zheng Z R, Shen J L, Ma Q, Chen H S, Jarillo-Herrero P and Dai S Y 2020 Configureurable phonon polaritons in twisted α-MoO_3 *Nat. Mater.* **19** 1307–11
[6] Lindsay L, Broido D A and Reinecke T L 2013 First-principles determination of ultrahigh thermal conductivity of boron arsenide: a competitor for diamond? *Phys. Rev. Lett.* **111** 025901
[7] Chiritescu C, Cahill D G, Nguyen N, Johnson D, Bodapati A, Keblinski P and Zschack P 2007 Ultralow thermal conductivity in disordered, layered WSe_2 crystals *Science* **315** 351–3
[8] Li N B, Ren J, Wang L, Zhang G, Hänggi P and Li B W 2012 *Colloquium*: phononics: manipulating heat flow with electronic analogs and beyond *Rev. Mod. Phys.* **84** 1045–66
[9] Chen X K, Pang M, Chen T, Du D and Chen K Q 2020 Thermal rectification in asymmetric graphene/hexagonal boron nitride van der Waals heterostructures *ACS Appl. Mater. Interfaces* **12** 15517–26
[10] Li B W, Wang L and Casati G 2006 Negative differential thermal resistance and thermal transistor *Appl. Phys. Lett.* **88** 143501
[11] Zhong W R, Huang W H, Deng X R and Ai B Q 2011 Thermal rectification in thickness-asymmetric graphene nanoribbons *Appl. Phys. Lett.* **99** 193104
[12] Wang Y, Chen S Y and Ruan X L 2012 Tunable thermal rectification in graphene nanoribbons through defect engineering: a molecular dynamics study *Appl. Phys. Lett.* **100** 163101
[13] Yang X M, Yu D P and Cao B Y 2017 Giant thermal rectification from single-carbon nanotube-graphene junction *ACS Appl. Mater. Interfaces* **9** 24078–84

[14] Zhang Y F, Lv Q, Wang H D, Zhao S Y, Xiong Q H, Lv R T and Zhang X 2022 Simultaneous electrical and thermal rectification in a monolayer lateral heterojunction *Science* **378** 169–75

[15] Sood A *et al* 2018 An electrochemical thermal transistor *Nat. Commun.* **9** 4510

[16] Xie R G, Bui C T, Varghese B, Zhang Q X, Sow C H, Li B W and Thong J T L 2011 An electrically tuned solid-state thermal memory based on metal-insulator transition of single-crystalline VO_2 nanobeams *Adv. Funct. Mater.* **21** 1602–7

[17] Chen Z W, Zhang X Y and Pei Y Z 2018 Manipulation of phonon transport in thermoelectrics *Adv. Mater.* **30** 1705617

[18] Zheng W W, Luo Y B, Liu Y, Shi J, Xiong R and Wang Z Y 2019 Synergistical tuning interface barrier and phonon propagation in Au-Sb_2Te_3 nanoplate for boosting thermoelectric performance *J. Phys. Chem. Lett.* **10** 4903–9

[19] Tang J Y, Wang H T, Lee D H, Fardy M, Huo Z Y, Russell T P and Yang P D 2010 Holey silicon as an efficient thermoelectric material *Nano Lett.* **10** 4279–83

[20] Schittny R, Kadic M, Guenneau S and Wegener M 2013 Experiments on transformation thermodynamics: molding the flow of heat *Phys. Rev. Lett.* **110** 195901

[21] Venema L, Verberck B, Georgescu I, Prando G, Couderc E, Milana S, Maragkou M, Persechini L, Pacchioni G and Fleet L 2016 The quasiparticle zoo *Nat. Phys.* **12** 1085–9

[22] Peierls R 1929 Zur kinetischen theorie der wärmeleitung in Kristallen *Ann. Phys.* **395** 1055–101

[23] Callaway J 1959 Model for lattice thermal conductivity at low temperatures *Phys. Rev.* **113** 1046–51

[24] Holland M G 1963 Analysis of lattice thermal conductivity *Phys. Rev.* **132** 2461–71

[25] Qian X, Zhou J W and Chen G 2021 Phonon-engineered extreme thermal conductivity materials *Nat. Mater.* **20** 1188–202

[26] Alder B J and Wainwright T E 1959 Studies in molecular dynamics. I. General method *J. Chem. Phys.* **31** 459–66

[27] Car R and Parrinello M 1985 Unified approach for molecular dynamics and density-functional theory *Phys. Rev. Lett.* **55** 2471–4

[28] Hu J N, Ruan X L and Chen Y P 2009 Thermal conductivity and thermal rectification in graphene nanoribbons: a molecular dynamics study *Nano Lett.* **9** 2730–5

[29] Lindsay L, Broido D A and Reinecke T L 2012 Thermal conductivity and large isotope effect in GaN from first principles *Phys. Rev. Lett.* **109** 095901

[30] Garg J, Bonini N, Kozinsky B and Marzari N 2011 Role of disorder and anharmonicity in the thermal conductivity of silicon-germanium alloys: a first-principles study *Phys. Rev. Lett.* **106** 045901

[31] Luo Y X, Yang X L, Feng T L, Wang J Y and Ruan X L 2020 Vibrational hierarchy leads to dual-phonon transport in low thermal conductivity crystals *Nat. Commun.* **11** 2554

[32] Stewart D A, Savić I and Mingo N 2009 First-principles calculation of the isotope effect on boron nitride nanotube thermal conductivity *Nano Lett.* **9** 81–84

[33] Oh D W, Jain A, Eaton J K, Goodson K E and Lee J S 2008 Thermal conductivity measurement and sedimentation detection of aluminum oxide nanofluids by using the 3ω method *Int. J. Heat Fluid Flow* **29** 1456–61

[34] Heron J S, Fournier T, Mingo N and Bourgeois O 2009 Mesoscopic size effects on the thermal conductance of silicon nanowire *Nano Lett.* **9** 1861–5

[35] Fujii M, Zhang X, Xie H Q, Ago H, Takahashi K, Ikuta T, Abe H and Shimizu T 2005 Measuring the thermal conductivity of a single carbon nanotube *Phys. Rev. Lett.* **95** 065502

[36] Ma W G, Miao T T, Zhang X, Takahashi K, Ikuta T, Zhang B P and Ge Z H 2016 A T-type method for characterization of the thermoelectric performance of an individual free-standing single crystal Bi_2S_3 nanowire *Nanoscale* **8** 2704–10

[37] Wang H D, Hu S Q, Takahashi K, Zhang X, Takamatsu H and Chen J 2017 Experimental study of thermal rectification in suspended monolayer graphene *Nat. Commun.* **8** 15843

[38] Zhao S Y and Wang H D 2020 An integrated H-type method to measure thermoelectric properties of two-dimensional materials *ES Energy Environ.* **9** 59–66

[39] Chen S S *et al* 2011 Raman measurements of thermal transport in suspended monolayer graphene of variable sizes in vacuum and gaseous environments *ACS Nano* **5** 321–8

[40] Xu S, Fan A R, Wang H D, Zhang X and Wang X W 2020 Raman-based nanoscale thermal transport characterization: a critical review *Int. J. Heat Mass Transfer* **154** 119751

[41] Li Q Y, Zhang X and Hu Y D 2014 Laser flash Raman spectroscopy method for thermophysical characterization of 2D nanomaterials *Thermochim. Acta* **592** 67–72

[42] Yuan P Y, Wang R D, Tan H, Wang T Y and Wang X W 2017 Energy transport state resolved Raman for probing interface energy transport and hot carrier diffusion in few-layered MoS_2 *ACS Photonics* **4** 3115–29

[43] Fan A R, Hu Y D, Wang H D, Ma W G and Zhang X 2019 Dual-wavelength flash Raman mapping method for measuring thermal diffusivity of suspended 2D nanomaterials *Int. J. Heat Mass Transfer* **143** 118460

[44] Zhang Z L, Sheng S X, Wang R M and Sun M T 2016 Tip-enhanced Raman spectroscopy *Anal. Chem.* **88** 9328–46

[45] Verma P 2017 Tip-enhanced Raman spectroscopy: technique and recent advances *Chem. Rev.* **117** 6447–66

[46] Zobeiri H, Hunter N, Xu S, Xie Y S and Wang X W 2022 Robust and high-sensitivity thermal probing at the nanoscale based on resonance Raman ratio (R3) *Int. J. Extrem. Manuf.* **4** 035201

[47] Yue Y N, Chen X W and Wang X W 2011 Noncontact sub-10 nm temperature measurement in near-field laser heating *ACS Nano* **5** 4466–75

[48] Huang D Z, Sun Q S, Liu Z Y, Xu S, Yang R G and Yue Y N 2023 Ballistic thermal transport at sub-10 nm laser-induced hot spots in GaN crystal *Adv. Sci.* **10** 2204777

[49] Ma W G, Miao T T, Zhang X, Kohno M and Takata Y 2015 Comprehensive study of thermal transport and coherent acoustic-phonon wave propagation in thin metal film-substrate by applying picosecond laser pump-probe method *J. Phys. Chem.* C **119** 5152–9

[50] Jiang P Q, Qian X and Yang R G 2018 Tutorial: time-domain thermoreflectance (TDTR) for thermal property characterization of bulk and thin film materials *J. Appl. Phys.* **124** 161103

[51] Qian X, Jiang P Q and Yang R G 2017 Anisotropic thermal conductivity of 4H and 6H silicon carbide measured using time-domain thermoreflectance *Mater. Today Phys.* **3** 70–75

[52] Eesley G L 1983 Observation of nonequilibrium electron heating in copper *Phys. Rev. Lett.* **51** 2140–3

[53] Jiang P Q, Qian X and Yang R G 2017 Time-domain thermoreflectance (TDTR) measurements of anisotropic thermal conductivity using a variable spot size approach *Rev. Sci. Instrum.* **88** 074901

[54] Li M, Kang J S and Hu Y J 2018 Anisotropic thermal conductivity measurement using a new asymmetric-beam time-domain thermoreflectance (AB-TDTR) method *Rev. Sci. Instrum.* **89** 084901

[55] Huxtable S, Cahill D G, Fauconnier V, White J O and Zhao J C 2004 Thermal conductivity imaging at micrometre-scale resolution for combinatorial studies of materials *Nat. Mater.* **3** 298–301

[56] Pek E K, Brethauer J and Cahill D G 2020 High spatial resolution thermal conductivity mapping of SiC/SiC composites *J. Nucl. Mater.* **542** 152519

[57] Wang M K, Ramer G, Perez-Morelo D J, Pavlidis G, Schwartz J J, Yu L Y, Ilic R, Aksyuk V A and Centrone A 2022 High throughput nanoimaging of thermal conductivity and interfacial thermal conductance *Nano Lett.* **22** 4325–32

[58] Jiang P Q, Huang B and Koh Y K 2016 Accurate measurements of cross-plane thermal conductivity of thin films by dual-frequency time-domain thermoreflectance (TDTR) *Rev. Sci. Instrum.* **87** 075101

[59] Slack G A 1973 Nonmetallic crystals with high thermal conductivity *J. Phys. Chem. Solids* **34** 321–35

[60] Ziman J M 2001 *Electrons and Phonons: The Theory of Transport Phenomena in Solids* (Oxford University Press)

[61] Shi X, Chen L and Uher C 2016 Recent advances in high-performance bulk thermoelectric materials *Int. Mater. Rev.* **61** 379–415

[62] Snyder G J, Christensen M, Nishibori E, Caillat T and Iversen B B 2004 Disordered zinc in Zn_4Sb_3 with phonon-glass and electron-crystal thermoelectric properties *Nat. Mater.* **3** 458–63

[63] Biswas K, He J Q, Zhang Q C, Wang G Y, Uher C, Dravid V P and Kanatzidis M G 2011 Strained endotaxial nanostructures with high thermoelectric figure of merit *Nat. Chem.* **3** 160–6

[64] Kargar F, Penilla E H, Aytan E, Lewis J S, Garay J E and Balandin A A 2018 Acoustic phonon spectrum engineering in bulk crystals via incorporation of dopant atoms *Appl. Phys. Lett.* **112** 191902

[65] Casimir H B G 1938 Note on the conduction of heat in crystals *Physica* **5** 495–500

[66] Li D Y, Wu Y Y, Kim P, Shi L, Yang P D and Majumdar A 2003 Thermal conductivity of individual silicon nanowires *Appl. Phys. Lett.* **83** 2934–6

[67] Cheaito R, Duda J C, Beechem T E, Hattar K, Ihlefeld J F, Medlin D L, Rodriguez M A, Campion M J, Piekos E S and Hopkins P E 2012 Experimental investigation of size effects on the thermal conductivity of silicon-germanium alloy thin films *Phys. Rev. Lett.* **109** 195901

[68] Balandin A and Wang K L 1998 Significant decrease of the lattice thermal conductivity due to phonon confinement in a free-standing semiconductor quantum well *Phys. Rev.* B **58** 1544–9

[69] Maire J, Anufriev R and Nomura M 2017 Ballistic thermal transport in silicon nanowires *Sci. Rep.* **7** 41794

[70] Siemens M E, Li Q, Yang R G, Nelson K A, Anderson E H, Murnane M M and Kapteyn H C 2010 Quasi-ballistic thermal transport from nanoscale interfaces observed using ultrafast coherent soft x-ray beams *Nat. Mater.* **9** 26–30

[71] Anufriev R, Ramiere A, Maire J and Nomura M 2017 Heat guiding and focusing using ballistic phonon transport in phononic nanostructures *Nat. Commun.* **8** 15505

[72] Anufriev R and Nomura M 2020 Ray phononics: thermal guides, emitters, filters, and shields powered by ballistic phonon transport *Mater. Today Phys.* **15** 100272

[73] Terraneo M, Peyrard M and Casati G 2002 Controlling the energy flow in nonlinear lattices: a model for a thermal rectifier *Phys. Rev. Lett.* **88** 094302

[74] Li B W, Wang L and Casati G 2004 Thermal diode: rectification of heat flux *Phys. Rev. Lett.* **93** 184301

[75] Wang L and Li B W 2007 Thermal logic gates: computation with phonons *Phys. Rev. Lett.* **99** 177208

[76] Wang L and Li B W 2008 Thermal memory: a storage of phononic information *Phys. Rev. Lett.* **101** 267203

[77] Starr C 1936 The copper oxide rectifier *Physics* **7** 15–19

[78] Roberts N A and Walker D G 2011 A review of thermal rectification observations and models in solid materials *Int. J. Therm. Sci.* **50** 648–62

[79] Rogers G F C 1961 Heat transfer at the interface of dissimilar metals *Int. J. Heat Mass Transfer* **2** 150–4

[80] Thomas T R and Probert S D 1970 Thermal contact resistance: the directional effect and other problems *Int. J. Heat Mass Transfer* **13** 789–807

[81] Marucha C, Mucha J and Rafałowicz J 1975 Heat flow rectification in inhomogeneous GaAs *Phys. Status Solidi* a **31** 269–73

[82] Jeżowski A and Rafalowicz J 1978 Heat flow asymmetry on a junction of quartz with graphite *Phys. Status Solidi* a **47** 229–32

[83] Hoff H 1985 Asymmetrical heat conduction in inhomogeneous materials *Physica* A **131** 449–64

[84] Lewis D V and Perkins H C 1968 Heat transfer at the interface of stainless steel and aluminum—the influence of surface conditions on the directional effect *Int. J. Heat Mass Transfer* **11** 1371–83

[85] Jones A, O'Callaghan P W and Probert S D 1971 Differential expansion thermal rectifier *J. Phys.* E **4** 438–40

[86] Wang Y, Vallabhaneni A, Hu J N, Qiu B, Chen Y P and Ruan X L 2014 Phonon lateral confinement enables thermal rectification in asymmetric single-material nanostructures *Nano Lett.* **14** 592–6

[87] Zhao S Y, Zhou Y H and Wang H D 2022 Review of thermal rectification experiments and theoretical calculations in 2D materials *Int. J. Heat Mass Transfer* **195** 123218

[88] Hu J N, Ruan X L and Chen Y P 2012 Molecular dynamics study of thermal rectification in graphene nanoribbons *Int. J. Thermophys.* **33** 986–91

[89] Zhang G and Zhang H S 2011 Thermal conduction and rectification in few-layer graphene Y junctions *Nanoscale* **3** 4604–7

[90] Yang X, Zheng X H, Liu Q S, Zhang T, Bai Y, Yang Z, Chen H S and Liu M 2020 Experimental study on thermal conductivity and rectification in suspended monolayer MoS_2 *ACS Appl. Mater. Interfaces* **12** 28306–12

[91] Kasprzak M, Sledzinska M, Zaleski K, Iatsunskyi I, Alzina F, Volz S, Torres C M S and Graczykowski B 2020 High-temperature silicon thermal diode and switch *Nano Energy* **78** 105261

[92] Chien S K, Yang Y T and Chen C K 2010 Thermal conductivity and thermal rectification in carbon nanotubes with geometric variations of doped nitrogen: non-equilibrium molecular dynamics simulations *Phys. Lett.* A **374** 4885–9

[93] Yuan K P, Sun M M, Wang Z L and Tang D W 2015 Tunable thermal rectification in silicon-functionalized graphene nanoribbons by molecular dynamics simulation *Int. J. Therm. Sci.* **98** 24–31

[94] Chen X K, Xie Z X, Zhang Y, Deng Y X, Zou T H, Liu J and Chen K Q 2019 Highly efficient thermal rectification in carbon/boron nitride heteronanotubes *Carbon* **148** 532–9

[95] Chen X K, Xie Z X, Zhou W X, Tang L M and Chen K Q 2016 Thermal rectification and negative differential thermal resistance behaviors in graphene/hexagonal boron nitride heterojunction *Carbon* **100** 492–500

[96] Chang C W, Okawa D, Majumdar A and Zettl A 2006 Solid-state thermal rectifier *Science* **314** 1121–4

[97] Gunawardana K G S H, Mullen K, Hu J N, Chen Y P and Ruan X L 2012 Tunable thermal transport and thermal rectification in strained graphene nanoribbons *Phys. Rev.* B **85** 245417

[98] Jiang P F, Hu S Q, Ouyang Y L, Ren W J, Yu C Q, Zhang Z W and Chen J 2020 Remarkable thermal rectification in pristine and symmetric monolayer graphene enabled by asymmetric thermal contact *J. Appl. Phys.* **127** 235101

[99] Zhao H B, Yang X, Wang C Y, Lu R, Zhang T, Chen H S and Zheng X H 2023 Progress in thermal rectification due to heat conduction in micro/nano solids *Mater. Today Phys.* **30** 100941

[100] Zhang Y Y, Pei Q X, Wang C M, Yang C H and Zhang Y W 2018 Interfacial thermal conductance and thermal rectification of hexagonal BC_nN/graphene in-plane heterojunctions *J. Phys. Chem.* C **122** 22783–9

[101] Zhuang S Y and Liu Y D 2020 Interface-controlled thermal rectification phenomenon of monolayer graphene/boron nitride heterosheet *J. Phys. Chem. Lett.* **11** 9731–7

[102] Sakai S, Samuelsen M R and Olsen O H 1987 Perturbation analysis of a parametrically changed sine-Gordon equation *Phys. Rev.* B **36** 217–25

[103] Woafo P 1998 Scattering of the φ^4 kink with an interface *Phys. Rev.* E **58** 1033–9

[104] Anderson P W 1958 Absence of diffusion in certain random lattices *Phys. Rev.* **109** 1492–505

[105] Luckyanova M N *et al* 2018 Phonon localization in heat conduction *Sci. Adv.* **4** eaat9460

[106] Hu J N, Wang Y, Vallabhaneni A, Ruan X L and Chen Y P 2011 Nonlinear thermal transport and negative differential thermal conductance in graphene nanoribbons *Appl. Phys. Lett.* **99** 113101

[107] Li F, Li H Y, Wang J, Xia G D and Hwang G 2022 Tunable thermal rectification and negative differential thermal resistance in gas-filled nanostructure with mechanically-controllable nanopillars *J. Therm. Sci.* **31** 1084–93

[108] Zhong W R, Zheng D Q and Hu B 2012 Thermal control in graphene nanoribbons: thermal valve, thermal switch and thermal amplifier *Nanoscale* **4** 5217–20

[109] Mazur A K and Maaloum M 2014 DNA flexibility on short length scales probed by atomic force microscopy *Phys. Rev. Lett.* **112** 068104

[110] Behnia S and Panahinia R 2018 Molecular thermal transistor: dimension analysis and mechanism *Chem. Phys.* **505** 40–46

[111] Chen F Q, Liu X J, Tian Y P, Wang D Y and Zheng Y 2021 Non-contact thermal transistor effects modulated by nanoscale mechanical deformation *J. Quant. Spectrosc. Radiat. Transfer* **259** 107414

[112] Saira O P, Meschke M, Giazotto F, Savin A M, Möttönen M and Pekola J P 2007 Heat transistor: demonstration of gate-controlled electronic refrigeration *Phys. Rev. Lett.* **99** 027203

[113] Yiğen S and Champagne A R 2014 Wiedemann-Franz relation and thermal-transistor effect in suspended graphene *Nano Lett.* **14** 289–93

[114] Vining C B 2001 Semiconductors are cool *Nature* **413** 577–8

[115] Xi H X, Luo L G and Fraisse G 2007 Development and applications of solar-based thermoelectric technologies *Renew. Sustain. Energy Rev.* **11** 923–36

[116] Burnete N V, Mariasiu F, Depcik C, Barabas I and Moldovanu D 2022 Review of thermoelectric generation for internal combustion engine waste heat recovery *Prog. Energy Combust. Sci.* **91** 101009

[117] Chen W Y, Shi X L, Zou J and Chen Z G 2022 Thermoelectric coolers for on-chip thermal management: materials, design, and optimization *Mater. Sci. Eng.* R **151** 100700

[118] Ren W *et al* 2021 High-performance wearable thermoelectric generator with self-healing, recycling, and Lego-like reconfiguring capabilities *Sci. Adv.* **7** eabe0586

[119] Shi X L, Zou J and Chen Z G 2020 Advanced thermoelectric design: from materials and structures to devices *Chem. Rev.* **120** 7399–515

[120] DiSalvo F J 1999 Thermoelectric cooling and power generation *Science* **285** 703–6

[121] Zheng Y *et al* 2015 Mechanically robust BiSbTe alloys with superior thermoelectric performance: a case study of stable hierarchical nanostructured thermoelectric materials *Adv. Energy Mater.* **5** 1401391

[122] Chang Z *et al* 2022 First-principles investigation of the significant anisotropy and ultrahigh thermoelectric efficiency of a novel two-dimensional $Ga_2I_2S_2$ at room temperature *Int. J. Extrem. Manuf.* **4** 025001

[123] Klemens P G 1955 The scattering of low-frequency lattice waves by static imperfections *Proc. Phys. Soc.* A **68** 1113–28

[124] Pei Y Z, Lensch-Falk J, Toberer E S, Medlin D L and Snyder G J 2011 High thermoelectric performance in PbTe due to large nanoscale Ag_2Te precipitates and la doping *Adv. Funct. Mater.* **21** 241–9

[125] Pei Y Z, Zheng L L, Li W, Lin S Q, Chen Z W, Wang Y Y, Xu X F, Yu H L, Chen Y and Ge B H 2016 Interstitial point defect scattering contributing to high thermoelectric performance in SnTe *Adv. Electron. Mater.* **2** 1600019

[126] Liu Z H, Mao J, Liu T H, Chen G and Ren Z F 2018 Nano-microstructural control of phonon engineering for thermoelectric energy harvesting *MRS Bull.* **43** 181–6

[127] Li W, Lin S Q, Zhang X Y, Chen Z W, Xu X F and Pei Y Z 2016 Thermoelectric properties of Cu_2SnSe_4 with intrinsic vacancy *Chem. Mater.* **28** 6227–32

[128] Zhang X Y, Li J, Wang X, Chen Z W, Mao J J, Chen Y and Pei Y Z 2018 Vacancy manipulation for thermoelectric enhancements in GeTe alloys *J. Am. Chem. Soc.* **140** 15883–8

[129] Rowe D M 2006 *Thermoelectrics Handbook: Macro to Nano* (CRC Press)

[130] Wu Y X *et al* 2020 Thermoelectric enhancements in PbTe alloys due to dislocation-induced strains and converged bands *Adv. Sci.* **7** 1902628

[131] Jiang Y *et al* 2022 Evolution of defect structures leading to high *ZT* in GeTe-based thermoelectric materials *Nat. Commun.* **13** 6087

[132] Xin J Z, Wu H J, Liu X H, Zhu T J, Yu G T and Zhao X B 2017 Mg vacancy and dislocation strains as strong phonon scatterers in $Mg_2Si_{1-x}Sb_x$ thermoelectric materials *Nano Energy* **34** 428–36

[133] Meng X F, Liu Z H, Cui B, Qin D D, Geng H Y, Cai W, Fu L W, He J Q, Ren Z F and Sui J 2017 Grain boundary engineering for achieving high thermoelectric performance in n-type skutterudites *Adv. Energy Mater.* **7** 1602582

[134] Xu L Q, Xiao Y, Wang S N, Cui B, Wu D, Ding X D and Zhao L D 2022 Dense dislocations enable high-performance PbSe thermoelectric at low-medium temperatures *Nat. Commun.* **13** 6449

[135] Fu C G, Wu H J, Liu Y T, He J Q, Zhao X B and Zhu T J 2016 Enhancing the figure of merit of heavy-band thermoelectric materials through hierarchical phonon scattering *Adv. Sci.* **3** 1600035

[136] Zwicky F 1932 Secondary structure and mosaic structure of crystals *Phys. Rev.* **40** 63–77

[137] Geis M W, Smith H I, Argoitia A, Angus J, Ma G H M, Glass J T, Butler J, Robinson C J and Pryor R 1991 Large-area mosaic diamond films approaching single-crystal quality *Appl. Phys. Lett.* **58** 2485–7

[138] He Y, Lu P, Shi X, Xu F F, Zhang T S, Snyder G J, Uher C and Chen L D 2015 Ultrahigh thermoelectric performance in mosaic crystals *Adv. Mater.* **27** 3639–44

[139] Lu B B, Wang M Y, Yang J, Hou H G, Zhang X Z, Shi Z Q, Liu J L, Qiao G J and Liu G W 2022 Dense twin and

domain boundaries lead to high thermoelectric performance in Sn-doped Cu_3SbS_4 *Appl. Phys. Lett.* **120** 173901
[140] Ying P J, Li X, Wang Y C, Yang J, Fu C G, Zhang W Q, Zhao X B and Zhu T J 2017 Hierarchical chemical bonds contributing to the intrinsically low thermal conductivity in α-MgAgSb thermoelectric materials *Adv. Funct. Mater.* **27** 1604145
[141] Hanus R, Agne M T, Rettie A J E, Chen Z W, Tan G J, Chung D Y, Kanatzidis M G, Pei Y Z, Voorhees P W and Snyder G J 2019 Lattice softening significantly reduces thermal conductivity and leads to high thermoelectric efficiency *Adv. Mater.* **31** 1900108
[142] Liu H L, Shi X, Xu F F, Zhang L L, Zhang W Q, Chen L D, Li Q, Uher C, Day T and Snyder G J 2012 Copper ion liquid-like thermoelectrics *Nat. Mater.* **11** 422–5
[143] He Y L, Shi X, Xu F F, Zhang L L, Zhang W Q, Chen L D, Li Q, Uher C, Day T and Snyder G J 2014 High thermoelectric performance in non-toxic earth-abundant copper sulfide *Adv. Mater.* **26** 3974–8
[144] Zhao K P, Qiu P F, Song Q F, Blichfeld A B, Eikeland E, Ren D D, Ge B H, Iversen B B, Shi X and Chen L D 2017 Ultrahigh thermoelectric performance in $Cu_{2-y}Se_{0.5}S_{0.5}$ liquid-like materials *Mater. Today Phys.* **1** 14–23
[145] Jakhar N, Bisht N, Katre A and Singh S 2022 Synergistic approach toward a reproducible high zT in n-type and p-type superionic thermoelectric Ag_2Te *ACS Appl. Mater. Interfaces* **14** 53916–27
[146] Lin Y *et al* 2020 Expression of interfacial Seebeck coefficient through grain boundary engineering with multi-layer graphene nanoplatelets *Energy Environ. Sci.* **13** 4114–21
[147] Hicks L D and Dresselhaus M S 1993 Thermoelectric figure of merit of a one-dimensional conductor *Phys. Rev.* B **47** 16631–4
[148] Yang X *et al* 2022 Progress in measurement of thermoelectric properties of micro/nano thermoelectric materials: a critical review *Nano Energy* **101** 107553
[149] Harman T C, Taylor P J, Walsh M P and LaForge B E 2002 Quantum dot superlattice thermoelectric materials and devices *Science* **297** 2229–32
[150] Li W, Zheng L L, Ge B H, Lin S Q, Zhang X Y, Chen Z W, Chang Y J and Pei Y Z 2017 Promoting SnTe as an eco-friendly solution for p-PbTe thermoelectric via band convergence and interstitial defects *Adv. Mater.* **29** 1605887
[151] Li J, Chen Z W, Zhang X Y, Yu H L, Wu Z H, Xie H Q, Chen Y and Pei Y Z 2017 Simultaneous optimization of carrier concentration and alloy scattering for ultrahigh performance GeTe thermoelectrics *Adv. Sci.* **4** 1700341
[152] Komatsu N, Ichinose Y, Dewey O S, Taylor L W, Trafford M A, Yomogida Y, Wehmeyer G, Pasquali M, Yanagi K and Kono J 2021 Macroscopic weavable fibers of carbon nanotubes with giant thermoelectric power factor *Nat. Commun.* **12** 4931
[153] Dresselhaus M S, Chen G, Tang M Y, Yang R G, Lee H, Wang D Z, Ren Z F, Fleurial J P and Gogna P 2007 New directions for low-dimensional thermoelectric materials *Adv. Mater.* **19** 1043–53
[154] Chang H T, Wang C C, Hsu J C, Hung M T, Li P W and Lee S W 2013 High quality multifold Ge/Si/Ge composite quantum dots for thermoelectric materials *Appl. Phys. Lett.* **102** 101902
[155] Vaziri S *et al* 2019 Ultrahigh thermal isolation across heterogeneously layered two-dimensional materials *Sci. Adv.* **5** eaax1325
[156] Venkatasubramanian R, Siivola E, Colpitts T and O'Quinn B 2001 Thin-film thermoelectric devices with high room-temperature figures of merit *Nature* **413** 597–602
[157] Kim W, Zide J, Gossard A, Klenov D, Stemmer S, Shakouri A and Majumdar A 2006 Thermal conductivity reduction and thermoelectric figure of merit increase by embedding nanoparticles in crystalline semiconductors *Phys. Rev. Lett.* **96** 045901
[158] Perez-Taborda J A, Muñoz Rojo M, Maiz J, Neophytou N and Martin-Gonzalez M 2016 Ultra-low thermal conductivities in large-area Si-Ge nanomeshes for thermoelectric applications *Sci. Rep.* **6** 32778
[159] Lee S, Kim K, Kang D H, Meyyappan M and Baek C K 2019 Vertical silicon nanowire thermoelectric modules with enhanced thermoelectric properties *Nano Lett.* **19** 747–55
[160] Wang Y, Huang H X and Ruan X L 2014 Decomposition of coherent and incoherent phonon conduction in superlattices and random multilayers *Phys. Rev.* B **90** 165406
[161] Xie G F, Ding D and Zhang G 2018 Phonon coherence and its effect on thermal conductivity of nanostructures *Adv. Phys.* X **3** 1480417
[162] Lee J, Lee W, Wehmeyer G, Dhuey S, Olynick D L, Cabrini S, Dames C, Urban J J and Yang P D 2017 Investigation of phonon coherence and backscattering using silicon nanomeshes *Nat. Commun.* **8** 14054
[163] Roy Chowdhury P, Reynolds C, Garrett A, Feng T L, Adiga S P and Ruan X L 2020 Machine learning maximized Anderson localization of phonons in aperiodic superlattices *Nano Energy* **69** 104428
[164] Venkatasubramanian R 2000 Lattice thermal conductivity reduction and phonon localizationlike behavior in superlattice structures *Phys. Rev.* B **61** 3091–7
[165] Liu W S, Yan X, Chen G and Ren Z F 2012 Recent advances in thermoelectric nanocomposites *Nano Energy* **1** 42–56
[166] Li J H, Tan Q, Li J F, Liu D W, Li F, Li Z Y, Zou M M and Wang K 2013 BiSbTe-based nanocomposites with high *ZT*: the effect of SiC nanodispersion on thermoelectric properties *Adv. Funct. Mater.* **23** 4317–23
[167] Zhao K P, Duan H Z, Raghavendra N, Qiu P F, Zeng Y, Zhang W Q, Yang J H, Shi X and Chen L D 2017 Solid-state explosive reaction for nanoporous bulk thermoelectric materials *Adv. Mater.* **29** 1701148
[168] Qiao J X, Zhao Y, Jin Q, Tan J, Kang S Q, Qiu J H and Tai K P 2019 Tailoring nanoporous structures in Bi_2Te_3 thin films for improved thermoelectric performance *ACS Appl. Mater. Interfaces* **11** 38075–83
[169] Hochbaum A I, Chen R K, Delgado R D, Liang W J, Garnett E C, Najarian M, Majumdar A and Yang P D 2008 Enhanced thermoelectric performance of rough silicon nanowires *Nature* **451** 163–7
[170] Zhao M L, Kim D, Lee Y H, Yang H and Cho S 2023 Quantum sensing of thermoelectric power in low-dimensional materials *Adv. Mater.* **35** 2106871
[171] Fan C Z, Gao Y and Huang J P 2008 Shaped graded materials with an apparent negative thermal conductivity *Appl. Phys. Lett.* **92** 251907
[172] Guenneau S, Amra C and Veynante D 2012 Transformation thermodynamics: cloaking and concentrating heat flux *Opt. Express* **20** 8207–18
[173] Han T C, Yuan T, Li B W and Qiu C W 2013 Homogeneous thermal cloak with constant conductivity and tunable heat localization *Sci. Rep.* **3** 1593
[174] Han T C, Bai X, Gao D L, Thong J T L, Li B W and Qiu C W 2014 Experimental demonstration of a bilayer thermal cloak *Phys. Rev. Lett.* **112** 054302
[175] Han T C, Bai X, Thong J T L, Li B W and Qiu C W 2014 Full control and manipulation of heat signatures: cloaking, camouflage and thermal metamaterials *Adv. Mater.* **26** 1731–4
[176] Sha W, Xiao M, Huang M Z and Gao L 2022 Topology-optimized freeform thermal metamaterials for

omnidirectionally cloaking sensors *Mater. Today Phys.* **28** 100880
[177] Ye Z Q and Cao B Y 2016 Nanoscale thermal cloaking in graphene via chemical functionalization *Phys. Chem. Chem. Phys.* **18** 32952–61
[178] Choe H S *et al* 2019 Ion write microthermotics: programing thermal metamaterials at the microscale *Nano Lett.* **19** 3830–7
[179] Liu Y D, Cheng Y H, Hu R and Luo X B 2019 Nanoscale thermal cloaking by *in-situ* annealing silicon membrane *Phys. Lett.* A **383** 2296–301
[180] Zhang J, Zhang H C, Zhang D, Sun W B and Li Y Y 2022 Performance investigation of nanoscale thermal cloak by the perforated silicon film *Curr. Appl. Phys.* **35** 38–44
[181] Little W A 1959 The transport of heat between dissimilar solids at low temperatures *Can. J. Phys.* **37** 334–49
[182] Swartz E T and Pohl R O 1989 Thermal boundary resistance *Rev. Mod. Phys.* **61** 605–68
[183] Kirkpatrick T R 1985 Localization of acoustic waves *Phys. Rev.* B **31** 5746–55
[184] Chen G 2021 Non-Fourier phonon heat conduction at the microscale and nanoscale *Nat. Rev. Phys.* **3** 555–69
[185] Joshi A A and Majumdar A 1993 Transient ballistic and diffusive phonon heat transport in thin films *J. Appl. Phys.* **74** 31–39
[186] Hsiao T K, Chang H K, Liou S C, Chu M W, Lee S C and Chang C W 2013 Observation of room-temperature ballistic thermal conduction persisting over 8.3 μm in SiGe nanowires *Nat. Nanotechnol.* **8** 534–8
[187] Wehmeyer G, Yabuki T, Monachon C, Wu J Q and Dames C 2017 Thermal diodes, regulators, and switches: physical mechanisms and potential applications *Appl. Phys. Rev.* **4** 041304
[188] Yamawaki M, Ohnishi M, Ju S H and Shiomi J 2018 Multifunctional structural design of graphene thermoelectrics by Bayesian optimization *Sci. Adv.* **4** eaar4192
[189] Li M, Dai L Y and Hu Y J 2022 Machine learning for harnessing thermal energy: from materials discovery to system optimization *ACS Energy Lett.* **7** 3204–26
[190] Hu R, Iwamoto S, Feng L, Ju S H, Hu S Q, Ohnishi M, Nagai N, Hirakawa K and Shiomi J 2020 Machine-learning-optimized aperiodic superlattice minimizes coherent phonon heat conduction *Phys. Rev.* X **10** 021050
[191] Lin S C, Liu Y X, Cai Z L and Zhao C Y 2023 High-throughput screening of aperiodic superlattices based on atomistic simulation-informed effective medium theory and genetic algorithm *Int. J. Heat Mass Transfer* **202** 123694
[192] Wang T, Zhang C, Snoussi H and Zhang G 2020 Machine learning approaches for thermoelectric materials research *Adv. Funct. Mater.* **30** 1906041
[193] Hou Z F, Takagiwa Y, Shinohara Y, Xu Y B and Tsuda K 2019 Machine-learning-assisted development and theoretical consideration for the $Al_2Fe_3Si_3$ thermoelectric material *ACS Appl. Mater. Interfaces* **11** 11545–54
[194] Ji Q X, Qi Y C, Liu C W, Meng S H, Liang J, Kadic M and Fang G D 2022 Design of thermal cloaks with isotropic materials based on machine learning *Int. J. Heat Mass Transfer* **189** 122716
[195] Ji Q X, Chen X Y, Liang J, Fang G D, Laude V, Arepolage T, Euphrasie S, Iglesias Martínez J A, Guenneau S and Kadic M 2022 Deep learning based design of thermal metadevices *Int. J. Heat Mass Transfer* **196** 123149
[196] Lu Q Y, Huberman S, Zhang H T, Song Q C, Wang J Y, Vardar G, Hunt A, Waluyo I, Chen G and Yildiz B 2020 Bi-directional tuning of thermal transport in $SrCoO_x$ with electrochemically induced phase transitions *Nat. Mater.* **19** 655–62
[197] Zhang L F, Wang J S and Li B W 2010 Ballistic thermal rectification in nanoscale three-terminal junctions *Phys. Rev.* B **81** 100301
[198] Maldovan M and Thomas E L 2006 Simultaneous localization of photons and phonons in two-dimensional periodic structures *Appl. Phys. Lett.* **88** 251907